AIAA JOURNAL
Vol. 48, No. 2, February 2010

Active Vibration Control of Flexible Rotors on Maneuvering Vehicles

A. S. Das*
National Institute of Technology Rourkela, Orissa 769 008, India
J. K. Dutt†
Indian Institute of Technology Delhi, New Delhi 110 016 India
and
K. Ray‡
Indian Institute of Technology Kharagpur, Kharagpur, West Bengal 721 302 India

DOI: 10.2514/1.43378

This paper presents a simulation to actively control transverse vibration of a flexible rotor shaft system mounted on a moving vehicle (e.g., a ship or an aircraft). Discretizing the rotor continuum with beam finite elements, equations of motion are written with respect to a noninertial frame attached to the frame of the moving vehicle. Such equations are linear but contain time-varying parametric terms due to the motion of the carrier vehicle. Through numerical simulation, it is shown that the transverse response in the bending vibration of the rotor shaft relative to the supporting structure is significantly influenced by the inertia force, as well as the parametric excitations due to vehicle motion. A control strategy is proposed using an electromagnetic actuator placed at a suitable location along the span of the rotor, and it is found extremely useful in reducing the vibration of the rotor and improving its stability. Examples are given in support by studying both the uncontrolled and the controlled motion of a rotor shaft system carried by an aircraft undergoing two different kinds of maneuvers.

Nomenclature

A_p	=	area of each pole face in the electromagnet, m^2
$[\boldsymbol{C}]_D$, $[\boldsymbol{C}]_S^e$	=	matrix to account for the Coriolis component of the acceleration for a disc and of a shaft finite element, respectively
$[\boldsymbol{D}]$	=	assembled matrix coefficient to the global velocity vector of the system
$[\boldsymbol{D}]_{\text{ac}}$	=	augmented matrix for the system due to damping provided by the electromagnetic actuator
$[\boldsymbol{D}]_{\text{brg}}$	=	augmented matrix for the system due to bearing damping
$\mathcal{D}_S^e$	=	Rayleigh dissipation function for a shaft finite element due to the viscous form of internal material damping
E	=	Young's modulus, Pa
e	=	unbalance eccentricity, m
F_Y, F_Z	=	linearized components of resultant electromagnetic force provided by the actuator along the Y_0 and Z_0 directions, respectively, N
$\{\boldsymbol{f}\}$	=	global load vector for the rotor-shaft-bearing system
$[\boldsymbol{G}]_D$, $[\boldsymbol{G}]_S^e$	=	gyroscopic matrices due to a disc and a shaft finite element, respectively
g	=	acceleration due to gravity, m/s^2
g_0	=	nominal radial air gap between a pole face and the rotor surface, m
H	=	maximum fall in height of the aircraft during dive, m
I	=	area moment of inertia of the shaft cross section about the neutral axis, m^4
I_p, I_d	=	polar and transverse mass moments of inertia of a disc, respectively, $kg \cdot m^2$
i_{cY}, i_{cZ}	=	control current in the coils around the electromagnet poles aligned along the Y_0 and Z_0 directions, respectively, A
i_p, i_d	=	polar and transverse mass moments of inertia for per unit length of the shaft, respectively, $kg \cdot m$
i_0	=	bias current, A
$[\boldsymbol{K}]$	=	assembled matrix coefficient to the global degrees of freedom vector of the system
$[\boldsymbol{K}]_{\text{ac}}$	=	augmented matrix for the system due to the stiffness effect provided by the electromagnetic actuator
$[\boldsymbol{K}]_{\text{brg}}$	=	augmented matrix for the system due to bearing stiffness
$[\boldsymbol{K}_B]_S^e$	=	stiffness matrix of a shaft finite element due to bending
$[\boldsymbol{K}_C]_S^e$	=	circulatory matrix of a shaft finite element due to internal material damping
$[\boldsymbol{K}_{pxx}]_D$	=	matrices for a disc associated with the parametric stiffness effect due to the motion of the rotor base
$[\boldsymbol{K}_{pxx}]_S^e$	=	matrices for a shaft finite element associated with the parametric stiffness effect due to the motion of the rotor base
k_g	=	power amplifier gain, A/V
k_i	=	force-current factor of the electromagnetic actuator, N/A
k_{mag}	=	magnetic exciter constant
k_p	=	position feedback gain, V/m
k_S	=	force-displacement factor of the electromagnetic actuator, N/m

Received 24 January 2009; revision received 17 September 2009; accepted for publication 3 October 2009.

*Assistant Professor, Department of Mechanical Engineering; anindya990052003@yahoo.com.
†Associate Professor, Department of Mechanical Engineering, Hauz Khas; jkdutt@mech.iitd.ernet.in (Corresponding Author).
‡Associate Professor, Department of Mechanical Engineering; raykr@mech.iitkgp.ernet.in.

k_v = velocity feedback gain, V · s/m
l = length of a shaft finite element, m
$[\boldsymbol{M}]$ = assembled inertia matrix for the rotor-shaft-bearing system
$[\boldsymbol{M}]_D$, $[\boldsymbol{M}]_S^e$ = inertia matrices for a disc and a shaft finite element, respectively
$[\boldsymbol{M}_R]_D$, $[\boldsymbol{M}_R]_S^e$ = rotary inertia matrices for a disc and a shaft finite element, respectively
$[\boldsymbol{M}_T]_D$, $[\boldsymbol{M}_T]_S^e$ = translatory inertia matrices for a disc and a shaft finite element, respectively
m = mass per unit length of the shaft, kg/m
m_D = mass of a disc, kg
m_U = point mass equivalent to the unbalanced mass placed at the outer radius of the disc, kg
N = number of coil turns around a pair of actuator poles
$\{\boldsymbol{Q}\}_{\text{brg}}$ = load vector due to the force exerted by the bearing on the rotor shaft system
$\{\boldsymbol{Q}\}_C$ = augmented control force vector
$\{\boldsymbol{Q}\}_D$, $\{\boldsymbol{Q}\}_S^e$ = external load vector for a disc and a shaft finite element, respectively
$\{\boldsymbol{q}\}$ = global degrees of freedom vector for the rotor-shaft-bearing system
$\{\boldsymbol{q}\}_D$, $\{\boldsymbol{q}\}_S^e$ = degrees of freedom vector associated with a disc and shaft finite element, respectively
$\bar{R}$ = position vector of the origin of the reference frame F_b, fixed to the rotor base, relative to the inertial frame of reference, m
$\bar{r}^C$ = position vector of any generic point C on the shaft axis, relative to the inertial frame of reference, m
$\{\boldsymbol{S}_{xx}\}_D$ = vectors associated with the inertia force acting on a disc due to the motion of the rotor base
$\{\boldsymbol{S}_{xx}\}_S^e$ = vectors associated with the inertia force acting on a shaft finite element due to the motion of the rotor base
$\mathcal{T}_D$, $\mathcal{T}_S^e$ = kinetic energy of a disc and a shaft finite element, respectively, J
$\mathcal{T}_U$ = kinetic energy associated with an unbalanced mass, J
t = time, s
u_a = component of absolute displacement of a generic point C on the shaft axis, measured along the axis OX_b of the frame F_b, fixed to the rotor base, m/s
$\mathcal{U}_D$, $\mathcal{U}_S^e$ = potential energy due to gravity of a disc and a shaft finite element, respectively, J
V = forward speed of the vehicle (e.g., aircraft), m/s
$\bar{V}^C$ = absolute velocity of a generic point C on the shaft axis, m/s
$\bar{V}^U$ = absolute velocity of an unbalanced mass, m/s
$V_{j_b}^b$ = components of the absolute velocity of the origin of the frame F_b, fixed to the base, along the OX_b, OY_b, and OZ_b axes, respectively ($j = X, Y, Z$), m/s
$V_{j_0}^G$ = components of the absolute velocity of the center of mass of the vehicle (e.g., aircraft) along the OX_0, OY_0, and OZ_0 axes, respectively ($j = X, Y, Z$), m/s
$\mathcal{V}_S^e$ = strain energy of a shaft finite element, J
v = component of displacement of a generic point on the shaft axis, along the direction of the Y_b axis, m
v_a = component of absolute displacement of a generic point C on the shaft axis, measured along the axis OY_b of the frame F_b, fixed to the rotor base, m
w = component of displacement of a generic point on the shaft axis, along the direction of the Z_b axis, m
w_a = component of absolute displacement of a generic point C on the shaft axis, measured along the axis OZ_b of the frame F_b, fixed to the rotor base, m
x = coordinate of a generic point along the length of the shaft, m
x_b^b = components of $\bar{R}$ along the axis OX_b of the reference frame F_b, fixed to the rotor base, m
${}_Gx^b$ = coordinate of the origin of the frame F_b, fixed to the rotor base, with respect to the center of mass of the vehicle, measured along the direction of OX_b, m
y_b^b = components of $\bar{R}$ along the axis OY_b of the reference frame F_b, fixed to the rotor base, m
${}_Gy^b$ = coordinate of the origin of the frame F_b, fixed to the rotor base, with respect to the center of mass of the vehicle, measured along the direction of OY_b, m
z_0^G = coordinate of the center of mass of the aircraft along the OZ_0 axis, m
z_b^b = components of $\bar{R}$ along the axis OZ_b of the reference frame F_b, fixed to the rotor base, m
${}_Gz^b$ = coordinate of the origin of the frame F_b, fixed to the rotor base, with respect to the center of mass of the vehicle, measured along the direction of OZ_b, m
z_0 = coordinate of the generic point C on the shaft, along Z_0 axis, m
α = half of the angle subtended by a pair of adjacent poles at the center of the rotor section, rad
α_P = angle of pitching, rad
B = rotation of the shaft cross section due to bending about the horizontal direction perpendicular to the shaft axis, at a generic location on the shaft, rad
β_Y = angle of yaw, rad
Γ = rotation of the shaft cross section due to bending about the vertical direction perpendicular to the shaft axis, at a generic location on the shaft, rad
γ = orientation of a generic fiber in the shaft cross section relative to the spin-synchronized reference frame, rad
γ_R = angle of rolling, rad
γ_U = phase angle of the unbalance eccentricity with respect to a horizontal transverse direction of the rotor, rad
$\hat{\varepsilon}_{j_0}$ = unit vector along the coordinate axes of the inertial reference frame, F_0 ($j = X, Y, Z$)
$\hat{\varepsilon}_{j_b}$ = unit vector along the coordinate axes of the frame F_b, fixed to the rotor base ($j = X, Y, Z$)
$\hat{\varepsilon}_{j_S}$ = unit vector along the coordinate axes of the frame F_S, fixed to a generic point of the rotor shaft system ($j = X, Y, Z$)
η_v = coefficient of the viscous form of the internal material damping of the shaft, s
λ = twice the length of the path over which the aircraft dives, m
μ_0 = absolute magnetic permeability of free air
ρ = radius of the curvature of the path along which the vehicle negotiates a turn, kg/m^3
$\bar{\rho}^C$ = position vector of a generic point C on the shaft axis, relative to the origin of the coordinate system attached to the frame F_b, fixed to the rotor base, m
Φ = angle of spin for the rotor, rad
$[\Psi]$ = shape function matrix

ψ_i = shape functions for a Rayleigh beam finite element ($i = 1, 2, 3, 4$)
Ω = spin speed, rad/s
$\bar{\Omega}_b$ = absolute angular velocity vector of the rotor base, rad/s
$\Omega^b_{j_b}$ = components of $\bar{\Omega}_b$ along the OX_b, OY_b, and OZ_b axes, respectively ($j = X, Y, Z$), rad/s
$\Omega^b_{j_S}$ = components of $\bar{\Omega}_b$ along the OX_S, OY_S, and OZ_S axes, respectively ($j = X, Y, Z$), rad/s
${}_b\bar{\Omega}^S$ = relative angular velocity vector of the cross section of the rotor shaft normal to the elastic line at a generic point C, with respect to the base, rad/s
${}_b\Omega^S_{j_S}$ = components of ${}_b\bar{\Omega}^S$ along the OX_S, OY_S, and OZ_S axes, respectively ($j = X, Y, Z$), rad/s
$\bar{\omega}$ = absolute angular velocity vector of the cross section of the rotor shaft normal to the elastic line at a generic point C, rad/s
ω_{j_S} = components of $\bar{\omega}$ along the OX_S, OY_S, and OZ_S axes, respectively ($j = X, Y, Z$), rad/s
$\omega^D_{j_S}$ = components of $\bar{\omega}^D$ along the OX_S, OY_S, and OZ_S axes, respectively ($j = X, Y, Z$), rad/s
$\bar{\omega}^D$ = angular velocity vector of the disc, rad/s

I. Introduction

ROTOR-SHAFT-BEARING systems (e.g., the gas turbine rotors of aeroengines, rotors of ship propulsion systems, rotors of generators carried in locomotives, etc.) may be classified as those working on moving bases and are subjected to inertia forces as well as parametric excitations due to the change of velocity under different maneuvering conditions in addition to other usual excitations. Studies in [1–12] primarily concentrated on finding the dynamic response of rotor-bearing systems due to seismic excitations. Influence of gyroscopic and Coriolis effects due to base rotation on the rotor response were particularly studied in [5,6]. Samali et al. [8] obtained the response of a rigid rotor on flexible bearings, considering the effect of parametric excitation caused by the rotation of the base. Su et al. [10] investigated seismic response of rotating machines, either rigidly attached to the floor or isolated by using a resilient-friction base isolator (RFBI). A response-spectrum-based approach was developed by Bachelet et al. [12] to investigate the dynamic behavior of an asymmetric rotor under random base excitation. Brown and Shabana [13] applied the principles of multibody dynamics to derive the equations of motion for flexible rotating shafts, in which coupling between base motion and deformation of the shaft was examined numerically, and the effect of the support motion on the dynamics of the shaft was discussed. Lin and Meng [14] studied the dynamics of a rotor carried within a maneuvering aircraft. Response of a single-disc rotor, running at a constant spin speed and constant angular acceleration, was determined numerically for maneuvering aircraft in a single vertical plane. Influence of aircraft flight parameters (i.e., aircraft velocity, acceleration, and flight path) on the rotor response was also investigated. Recently, Duchemin et al. [15] presented analytical as well as experimental studies on the dynamic behavior of a flexible rotor subjected to sinusoidal rotation of the support. The method of multiple scales was applied to identify the zones of instability of the rotor shaft system due to the presence of time-varying terms in the stiffness matrix. Driot et al. [16] reported studies with numerical as well as experimental verifications, in which the method of normal form was used to analytically examine the dynamics of a parametrically excited rotor.

Although situations in which rotor shaft systems are acted upon by inertia forces due to base motion are very common, a few reports were found to deal with the strategies to attenuate the rotor vibration initiated by such excitations. Cole et al. [17] reported the use of active magnetic bearings (AMBs) to attenuate the lateral vibration of a rotor under excitations due to mass unbalance and an initial impact at the base; however, the equations were derived with respect to a fixed reference frame. Matsushita et al. [11] showed the efficiency of an AMB with a feedforward control strategy to mitigate the rotor vibration under simulated seismic excitation. Keogh et al. [18] proposed a combined wavelet–H_∞ controller to attenuate the transient vibration and transmitted forces caused by unbalance and base motion.

This work presents a scheme and simulation results on actively controlling transverse rotor vibration of a flexible rotor with respect to the floor of a maneuvering vehicle, such as an aircraft in flight. The control action is applied by placing an actuator (consisting of four electromagnetic exciters of two poles each), reported by Nighil et al. [19] after following Janik and Irretier [20,21], integrally with the rotor base at a suitable location away from the bearings. The actuator generates a control force on the rotor section, proportional to the distance of the section from the poles and its time rate, over an air gap along two perpendicular directions on the rotor section. The actuator does not levitate the rotor or facilitate the bearing action, as it is supported on conventional bearings. Das et al. [22] studied the efficacy of such an actuator and its placement on controlling the unbalanced response of a flexible rotor and its stability. However, the influence of base excitation was not taken into account. Equations of motion of the rotor continuum, discretized with beam finite elements, are written with respect to the moving reference frame after considering the gyroscopic effect and internal damping of the rotor material. Numerical simulations are carried out to study the effectiveness of the electromagnetic actuator in actively controlling the transverse response of a flexible rotor shaft relative to the moving base. It has been observed that the actuator reduces flexural vibration of the rotor relative to the rotor base remarkably and, at the same time, safeguards the rotor against the onset of instability due to internal material damping. However, the mathematical analysis of stability due to parametric excitation (investigated by Das [23]) has not been addressed here to keep the paper short. With the same numerical model, further studies may be carried out to investigate the rotor response and means of its attenuation under more complicated conditions of maneuver, like Dutch roll, phugoid, and short period pitching mode for aircraft, as well as pitching and rolling of marine vessels.

II. Equations of Motion

A. Reference Frame and Kinematics

To derive the equations of motion of the flexible rotor-shaft-bearing system mounted on a maneuvering vehicle, the following three sets of coordinate axes are considered attached to three different reference frames (Fig. 1):

1) X_0–Y_0–Z_0 is fixed to the inertial frame of reference (F_0).

2) X_b–Y_b–Z_b is fixed to the rotor base (frame F_b), which in turn is fixed to the frame of the vehicle and, with the origin, coincident at the location of one of the bearings (e.g., the left bearing).

3) X_S–Y_S–Z_S is fixed to the rotor shaft at a generic point, rotating with it (frame F_S). The shaft axis is directed along X_S.

The position vector of any generic point C, situated on the shaft axis at a distance of x from the origin of the base-fixed coordinate system, is defined as

$$\bar{r}^{\,C}(x) = \bar{R} + \bar{\rho}^C \tag{1}$$

$\bar{R}$ is the absolute position vector of the origin of the base-fixed frame F_b, and $\bar{\rho}^C$ is the position vector of point C from the origin of the coordinate system attached to the frame F_b. Considering that the rotor shaft is sufficiently rigid in axial direction when compared with the transverse direction, $\bar{\rho}^C$ is expressed as

$$\bar{\rho}^{\,C}(x) = x\hat{\varepsilon}_{X_b} + v(x)\hat{\varepsilon}_{Y_b} + w(x)\hat{\varepsilon}_{Z_b} \tag{2}$$

where $\hat{\varepsilon}_{j_b}$ ($j = X, Y, Z$) are the unit vectors along the directions of OX_b, OY_b, and OZ_b, respectively. Components of the transverse deflection due to bending of the elastic line of the shaft relative to the

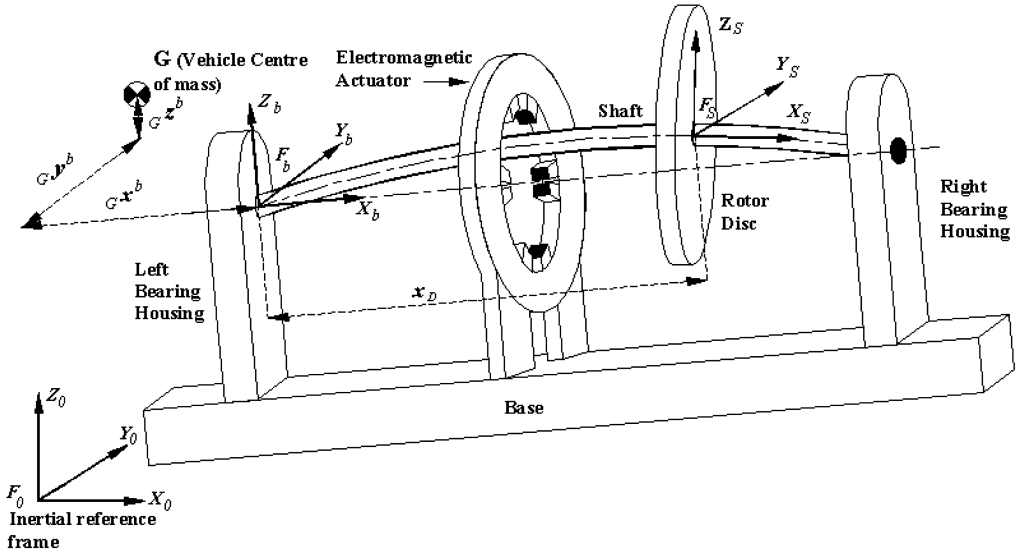

Fig. 1 Rotor-bearing system on moving base with different coordinate systems.

base along the OY_b and OZ_b axes are $v(x)$ and $w(x)$, respectively. To discretize the rotor shaft continuum, two-node Rayleigh beam finite elements (shown in Fig. 2) [24] are used. The degrees of freedom are given by the vector:

$$\{\boldsymbol{q}\}_S^e = [\,v_1 \quad w_1 \quad \mathrm{B}_1 \quad \Gamma_1 \quad v_2 \quad w_2 \quad \mathrm{B}_2 \quad \Gamma_2\,]^T \tag{3}$$

The relative transverse displacement components of a point on the shaft elastic line within the element are interpolated as

$$[\,v \quad w\,]^T = [\Psi]\{\boldsymbol{q}\}_S^e \tag{4}$$

Similarly, slopes of the elastic line relative to the rotor base at a point within the shaft finite element are interpolated as

$$[\,\mathrm{B} \quad \Gamma\,]^T = [\,-w' \quad v'\,]^T = \begin{bmatrix} 0 & -1 \\ 1 & 0 \end{bmatrix}[\Psi']\{\boldsymbol{q}\}_S^e \tag{5}$$

Elements of the shape function matrix $[\Psi]$ are given in the Appendix.

The absolute velocity of the point C is given by

$$\bar{V}^C = \dot{\bar{R}} + \bar{\Omega}^b \times \bar{\rho}^C + (\dot{v}\hat{\varepsilon}_{Y_b} + \dot{w}\hat{\varepsilon}_{Z_b}) = \dot{u}_a\hat{\varepsilon}_{X_b} + \dot{v}_a\hat{\varepsilon}_{Y_b} + \dot{w}_a\hat{\varepsilon}_{Z_b} \tag{6}$$

where $\dot{u}_a$, $\dot{v}_a$, and $\dot{w}_a$ [expressed in Eqs. (7)] are the absolute velocity components of the point C along OX_b, OY_b, and OZ_b, respectively, and $\bar{\Omega}^b$ is the absolute angular velocity vector of the rotor base:

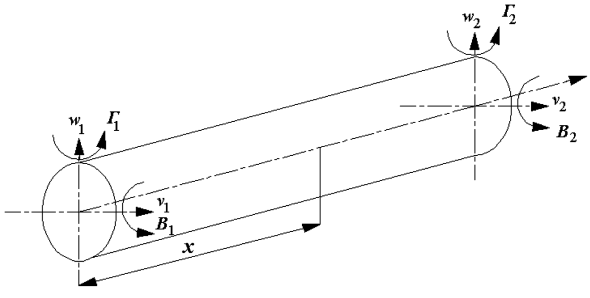

Fig. 2 Rayleigh beam finite element.

$$\left.\begin{aligned} \dot{u}_a &= (V^b_{X_b} + \Omega^b_{Y_b} w - \Omega^b_{Z_b} v) \\ \dot{v}_a &= (V^b_{Y_b} - \Omega^b_{X_b} w + \Omega^b_{Z_b} x + \dot{v}) \\ \dot{w}_a &= (V^b_{Z_b} + \Omega^b_{X_b} v - \Omega^b_{Y_b} x + \dot{w}) \end{aligned}\right\} \tag{7}$$

In the previous expressions, $V^b_{j_b}(j = X, Y, Z)$ are the components of the absolute velocity of the origin of F_b along the OX_b, OY_b, and OZ_b axes, respectively, and are evaluated from the velocity components of the vehicle and the coordinates of the origin of the frame F_b with respect to some reference point inside the vehicle (e.g., the center of mass of the vehicle). The components of vector $\bar{\Omega}^b$ along OX_b, OY_b, and OZ_b are denoted as $\Omega^b_{j_b}(j = X, Y, Z)$.

The absolute angular velocity vector of the cross section of the rotor shaft normal to the elastic line at point C is given by

$$\bar{\omega} = \bar{\Omega}^b + {}_b\bar{\Omega}^S = \omega_{X_S}\hat{\varepsilon}_{X_S} + \omega_{Y_S}\hat{\varepsilon}_{Y_S} + \omega_{Z_S}\hat{\varepsilon}_{Z_S} \tag{8}$$

where $\hat{\varepsilon}_{j_S}(j = X, Y, Z)$ are the unit vectors and $\omega_{j_S}(j = X, Y, Z)$ (given in the Appendix) are the components of $\bar{\omega}$, along the OX_S, OY_S, and OZ_S axes, respectively. The angular velocity vector of the cross section at point C relative to the base ${}_b\bar{\Omega}^S$ is given by

$${}_b\bar{\Omega}^S = {}_b\Omega^S_{X_S}\hat{\varepsilon}_{X_S} + {}_b\Omega^S_{Y_S}\hat{\varepsilon}_{Y_S} + {}_b\Omega^S_{Z_S}\hat{\varepsilon}_{Z_S} \tag{9}$$

where

$$\left.\begin{aligned} {}_b\Omega^S_{X_S} &= \dot{\Phi} - \dot{\Gamma}\sin\mathrm{B} \\ {}_b\Omega^S_{Y_S} &= \dot{\Gamma}\sin\Phi\cos\mathrm{B} + \dot{\mathrm{B}}\cos\Phi \\ {}_b\Omega^S_{Z_S} &= \dot{\Gamma}\cos\Phi\cos\mathrm{B} - \dot{\mathrm{B}}\sin\Phi \end{aligned}\right\} \tag{10}$$

In the previous expressions, $\dot{\Gamma}$ and $\dot{\mathrm{B}}$ are the rates of change of the slopes of the elastic line at point C relative to the base along the OY_b and OZ_b axes, respectively, Ω is the spin speed of the rotor, and t is the time elapsed.

B. Equations of Motion for a Rotor Disc Element

The expression of kinetic energy of a rotor disc situated at a distance of x_D from the origin of F_b (as shown in Fig. 1) is given by

$$\mathcal{T}_D = \tfrac{1}{2}m_D[\dot{u}_a^2(x_D) + \dot{v}_a^2(x_D) + \dot{w}_a^2(x_D)] + \tfrac{1}{2}[I_P\omega_{X_S}^2(x_D) + I_D\{\omega_{Y_S}^2(x_D) + \omega_{Z_S}^2(x_D)\}] = \tfrac{1}{2}[m_D(\dot{v}_D^2 + \dot{w}_D^2) + I_d(\dot{\mathrm{B}}_D^2 + \dot{\Gamma}_D^2)] - (\dot{\Phi} + \Omega_{X_b}^b)I_p\dot{\Gamma}_D\mathrm{B}_D - \Omega_{X_b}^b[m_D(\dot{v}_D w_D - v_D\dot{w}_D) + I_d(\dot{\mathrm{B}}_D\Gamma_D - \mathrm{B}_D\dot{\Gamma}_D)] + \tfrac{1}{2}\Omega_{X_b}^{b^2}[m(v_D^2 + w_D^2) + i_d(\mathrm{B}_D^2 + \Gamma_D^2)] + \tfrac{1}{2}\Omega_{Z_b}^{b^2}[m_D v_D^2 + I_p\mathrm{B}_D^2] + \tfrac{1}{2}\Omega_{Y_b}^{b^2}[m_D w_D^2 + I_p\Gamma_D^2] - \Omega_{Y_b}^b\Omega_{Z_b}^b[m_D v_D w_D + (I_p - I_d)\mathrm{B}_D\Gamma_D] + \Omega_{Z_b}^b[m_D x_D\dot{v}_D + I_d\dot{\Gamma}_D] - \Omega_{Y_b}^b[m_D x_D\dot{w}_D - I_d\dot{\mathrm{B}}_D] + m_D[V_{Y_b}^b\dot{v}_D + V_{Z_b}^b\dot{w}_D] - \Omega_{X_b}^b\Omega_{Y_b}^b[m_D x_D v_D - (I_p - I_d)\Gamma_D] - \Omega_{X_b}^b\Omega_{Z_b}^b[m_D x_D w_D + (I_p - I_d)\mathrm{B}_D] + m_D[(V_{X_b}^b\Omega_{Z_b}^b - V_{Z_b}^b\Omega_{X_b}^b)v_D - (V_{X_b}^b\Omega_{Y_b}^b - V_{Y_b}^b\Omega_{X_b}^b)w_D] - \dot{\Phi}I_p[\Omega_{Z_b}^b\mathrm{B}_D - \Omega_{Y_b}^b\Gamma_D] + \tfrac{1}{2}[I_d(\Omega_{Y_b}^{b^2} + \Omega_{Z_b}^{b^2}) + I_p(\dot{\Phi} + \Omega_{X_b}^b)^2] + \tfrac{1}{2}m_D[V_{X_b}^{b^2} + V_{Y_b}^{b^2} + V_{Z_b}^{b^2} + 2x_D(V_{Y_b}^b\Omega_{Z_b}^b - V_{Z_b}^b\Omega_{Y_b}^b) + x_D^2(\Omega_{Y_b}^{b^2} + \Omega_{Z_b}^{b^2})] \tag{11}$$

In the previous equation, v_D and w_D are the transverse displacement components of the shaft relative to the rotor base along the OY_b and OZ_b axes, and B_D and Γ_D are the respective slopes of the elastic line of the shaft relative to the base in the X_b–Z_b plane and the X_b–Y_b plane at the disc location. The vector $\{q\}_D = [\,v_D \quad w_D \quad \mathrm{B}_D \quad \Gamma_D\,]^T$ represents the degrees of freedom at the disc node. The disc mass and the transverse and polar mass moments of inertia are denoted by m_D, I_d, and I_p, respectively.

To account for the potential energy due to disc weight, the relationship between the unit vector along the Z_0 axis of the inertial reference frame and the unit vectors of the base-fixed coordinate system (F_b) has to be found. For this purpose, it is assumed that the instantaneous configuration of the vehicle (hence, of the rotor base) can be reached through three successive Euler angle rotations (viz., α_P about the Y_b axis and β_Y and γ_R, respectively, about the instantaneous orientations of the Z_b and X_b axes) to simulate the pitching, yawing, and rolling motions. Letting z_0 be the coordinate of the generic point C on the shaft along the Z_0 axis, and letting x_b^b, y_b^b, and z_b^b be the components of $\bar{R}$ along the OX_b, OY_b, and OZ_b, respectively, z_0 can be expressed as in

$$z_0(x) = -(x_b^b + x)(\sin\alpha_P\cos\beta_Y) + (y_b^b + v)(\cos\alpha_P\sin\gamma_R + \sin\alpha_P\sin\beta_Y\cos\gamma_R) + (z_b^b + w)(\cos\alpha_P\cos\gamma_R - \sin\alpha_P\sin\beta_Y\sin\gamma_R) \tag{12}$$

Potential energy due to gravity of a disc at point C is given by

$$\mathcal{U}_D = m_D g z_0(x_D) \tag{13}$$

where $z_0(x_D)$ is the value of z_0 evaluated at $x = x_D$.

Following Lagrange's principle, the equation of motion (14) for a disc element is obtained using Eqs. (11) and (13):

$$[\boldsymbol{M}]_D\{\ddot{\boldsymbol{q}}\}_D - \{(\dot{\Phi} + \Omega_{X_b}^b)[\boldsymbol{G}]_D - 2\Omega_{X_b}^b[\boldsymbol{C}]_D\}\{\dot{\boldsymbol{q}}\}_D - \{(\ddot{\Phi} + \dot{\Omega}_{X_b}^b)[\boldsymbol{H}]_D - \dot{\Omega}_{X_b}^b[\boldsymbol{C}]_D\}\{\boldsymbol{q}\}_D - \{\Omega_{X_b}^{b^2}[\boldsymbol{M}]_D + \Omega_{Z_b}^{b^2}[\boldsymbol{K}_{p11}]_D + \Omega_{Y_b}^{b^2}[\boldsymbol{K}_{p22}]_D - \Omega_{Y_b}^b\Omega_{Z_b}^b[\boldsymbol{K}_{p12}]_D\}\{\boldsymbol{q}\}_D = -(\dot{\Omega}_{Z_b}^b + \Omega_{X_b}^b\Omega_{Y_b}^b)\{\boldsymbol{S}_{2Y}\}_D + (\dot{\Omega}_{Y_b}^b - \Omega_{X_b}^b\Omega_{Z_b}^b)\{\boldsymbol{S}_{2P}\}_D - (\dot{\Phi} + \Omega_{X_b}^b)\{\Omega_{Z_b}^b\{\boldsymbol{S}_{1P}\}_D - \Omega_{Y_b}^b\{\boldsymbol{S}_{1Y}\}_D\} - (\dot{V}_{Y_b}^b + V_{X_b}^b\Omega_{Z_b}^b - V_{Z_b}^b\Omega_{X_b}^b)\{\boldsymbol{S}_1\}_D - (\dot{V}_{Z_b}^b - V_{X_b}^b\Omega_{Y_b}^b + V_{Y_b}^b\Omega_{X_b}^b)\{\boldsymbol{S}_2\}_D - g(\cos\alpha_P\sin\gamma_R + \sin\alpha_P\sin\beta_Y\cos\gamma_R)\{\boldsymbol{S}_1\}_D - g(\cos\alpha_P\cos\gamma_R - \sin\alpha_P\sin\beta_Y\sin\gamma_R)\{\boldsymbol{S}_2\}_D + \{\boldsymbol{Q}\}_D \tag{14}$$

The expressions and implications of the different matrices (e.g., inertia, gyroscopic, Coriolis, and parametric stiffness matrices) and vectors are given in the Appendix.

C. Equation of Motion for a Shaft Finite Element

The kinetic energy of a differential portion of the shaft element, which is an infinitesimally thin disc of thickness dx, is given by

$$d\mathcal{T}_S^e = \tfrac{1}{2}m\{\dot{u}_a^2(x) + \dot{v}_a^2(x) + \dot{w}_a^2(x)\}dx + \tfrac{1}{2}\{i_p\omega_{X_S}^2(x) + i_d\omega_{Y_S}^2(x) + i_d\omega_{Z_S}^2(x)\}dx \tag{15}$$

where m is the mass, and i_d and i_p are the transverse and polar mass moments of inertia per unit length of the shaft element. By substituting different components of translational and rotational velocities, neglecting the exponent of the slopes more than two (as the slopes are supposed to be very small), and integrating Eq. (15) over the length of an element l, the expression of the kinetic energy is obtained as

$$\mathcal{T}_S^e = \frac{1}{2}\int_0^l [m(\dot{v}^2 + \dot{w}^2) + i_d(\dot{\mathrm{B}}^2 + \dot{\Gamma}^2)]\,\mathrm{d}x - (\dot{\Phi} + \Omega_{X_b}^b)\int_0^l i_p\dot{\Gamma}\mathrm{B}\,\mathrm{d}x - \Omega_{X_b}^b\int_0^l [m(\dot{v}w - v\dot{w}) + i_d(\dot{\mathrm{B}}\Gamma - \mathrm{B}\dot{\Gamma})]\mathrm{d}x + \frac{1}{2}\Omega_{X_b}^{b^2}\int_0^l [m(v^2 + w^2) + i_d(\mathrm{B}^2 + \Gamma^2)]\,\mathrm{d}x + \frac{1}{2}\Omega_{Z_b}^{b^2}\int_0^l [mv^2 + i_p\mathrm{B}^2]\,\mathrm{d}x + \frac{1}{2}\Omega_{Y_b}^{b^2}\int_0^l [mw^2 + i_p\Gamma^2]\,\mathrm{d}x - \Omega_{Y_b}^b\Omega_{Z_b}^b \times \int_0^l [mvw + (i_p - i_d)\mathrm{B}\Gamma]\,\mathrm{d}x + \Omega_{Z_b}^b\int_0^l [mx\dot{v} + i_d\dot{\Gamma}]\,\mathrm{d}x + \Omega_{Y_b}^b\int_0^l [mx\dot{w} + i_d\dot{\mathrm{B}}]\,\mathrm{d}x + \int_0^l m[V_{Y_b}^b\dot{v} + V_{Z_b}^b\dot{w}]\,\mathrm{d}x - \Omega_{X_b}^b\Omega_{Y_b}^b\int_0^l [mxv - (i_p - i_d)\Gamma]\,\mathrm{d}x - \Omega_{X_b}^b\Omega_{Z_b}^b\int_0^l [mxw + (i_p - i_d)\mathrm{B}]\,\mathrm{d}x + \int_0^l m[(V_{X_b}^b\Omega_{Z_b}^b - V_{Z_b}^b\Omega_{X_b}^b)v - (V_{X_b}^b\Omega_{Y_b}^b - V_{Y_b}^b\Omega_{X_b}^b)w]\,\mathrm{d}x - \dot{\Phi}\int_0^l i_p[\Omega_{Z_b}^b\mathrm{B} - \Omega_{Y_b}^b\Gamma]\mathrm{d}x + \frac{1}{2}\int_0^l [i_d(\Omega_{Y_b}^{b^2} + \Omega_{Z_b}^{b^2}) + i_p(\dot{\Phi} + \Omega_{X_b}^b)^2]\,\mathrm{d}x + \frac{1}{2}\int_0^l m[V_{X_b}^{b^2} + V_{Y_b}^{b^2} + V_{Z_b}^{b^2} + 2x(V_{Y_b}^b\Omega_{Z_b}^b - V_{Z_b}^b\Omega_{Y_b}^b) + x^2(\Omega_{Y_b}^{b^2} + \Omega_{Z_b}^{b^2})]\,\mathrm{d}x \tag{16}$$

Strain energy due to bending $\mathcal{V}_S^e$ and the Rayleigh dissipation function $\mathcal{D}_S^e$ due to the viscous form of internal material damping [25] for the shaft element are written as

$$\mathcal{V}_S^e = \frac{1}{2}\int_0^l EI(\mathrm{B}'^2 + \Gamma'^2)\,\mathrm{d}x \tag{17}$$

$$\mathcal{D}_S^e = \frac{1}{2}\eta_v\int_0^l EI\{(\dot{\Gamma}' - \dot{\Phi}\mathrm{B}')^2 + (\dot{\mathrm{B}}' + \dot{\Phi}\Gamma')^2\}\,\mathrm{d}x \tag{18}$$

where E and η_v are, respectively, the Young's modulus and the coefficient of viscous form of internal damping of the shaft material. I is the area moment of inertia of the shaft cross section about the neutral axis.

Following Eqs. (12) and (13), the potential energy due to gravity of the shaft element is given by

$$\mathcal{U}_S^e = \int_0^l mgz_0(x)\,\mathrm{d}x \tag{19}$$

Using the finite element interpolation functions [Eqs. (4) and (5)] and the expressions of the kinetic energy, strain energy, and dissipation functions, as well as the potential energy due to gravity [Eqs. (16–19)], the equations of motion are obtained from Lagrange's principle and are given in Eq. (20):

$$
\begin{aligned}
&[\boldsymbol{M}]^e_S\{\ddot{\boldsymbol{q}}\}^e_S - \{(\dot{\Phi}+\Omega^b_{X_b})[\boldsymbol{G}]^e_S - 2\Omega^b_{X_b}[\boldsymbol{C}]^e_S\}\{\dot{\boldsymbol{q}}\}^e_S - \{(\ddot{\Phi}+\dot{\Omega}^b_{X_b})[\boldsymbol{H}]^e_S \\
&\quad - \dot{\Omega}^b_{X_b}[\boldsymbol{C}]^e_S\}\{\boldsymbol{q}\}^e_S - \{\Omega^{b^2}_{X_b}[\boldsymbol{M}]^e_S + \Omega^{b^2}_{Z_b}[\boldsymbol{K}_{p11}]^e_S + \Omega^{b^2}_{Y_b}[\boldsymbol{K}_{p22}]^e_S \\
&\quad - \Omega^b_{Y_b}\Omega^b_{Z_b}[\boldsymbol{K}_{p12}]^e_S\}\{\boldsymbol{q}\}^e_S + \eta_v[\boldsymbol{K}_B]^e_S\{\dot{\boldsymbol{q}}\}^e_S + \{[\boldsymbol{K}_B]^e_S \\
&\quad + \eta_v\dot{\Phi}[\boldsymbol{K}_C]^e_S\}\{\boldsymbol{q}\}^e_S = -(\dot{\Omega}^b_{Z_b} + \Omega^b_{X_b}\Omega^b_{Y_b})\{\boldsymbol{S}_{2Y}\}^e_S \\
&\quad + (\dot{\Omega}^b_{Y_b} - \Omega^b_{X_b}\Omega^b_{Z_b})\{\boldsymbol{S}_{2P}\}^e_S - (\dot{\Phi}+\Omega^b_{X_b})[\Omega^b_{Z_b}\{\boldsymbol{S}_{1P}\}^e_S \\
&\quad - \Omega^b_{Y_b}\{\boldsymbol{S}_{1Y}\}^e_S] - (\dot{V}^b_{Y_b} + V^b_{X_b}\Omega^b_{Z_b} - V^b_{Z_b}\Omega^b_{X_b})\{\boldsymbol{S}_1\}^e_S \\
&\quad - (\dot{V}^b_{Z_b} - V^b_{X_b}\Omega^b_{Y_b} + V^b_{Y_b}\Omega^b_{X_b})\{\boldsymbol{S}_2\}^e_S - g(\cos\alpha_P\sin\gamma_R \\
&\quad + \sin\alpha_P\sin\beta_Y\cos\gamma_R)\{\boldsymbol{S}_1\}^e_S - g(\cos\alpha_P\cos\gamma_R \\
&\quad - \sin\alpha_P\sin\beta_Y\sin\gamma_R)\{\boldsymbol{S}_2\}^e_S + \{\boldsymbol{Q}\}^e_S
\end{aligned}
\tag{20}
$$

A detailed description of the different matrices (e.g. inertia, gyroscopic effect, Coriolis component, bending stiffness, circulatory, and parametric stiffness matrices) and vectors are given in the Appendix.

D. Equations of Motion for Concentrated Mass Unbalance Associated with a Disc

The mass unbalance associated with a disc is considered as a concentrated mass m_U at a point with the eccentricity e and the initial phase angle γ_U. Kinetic energy of the unbalanced mass is written as

$$
\mathcal{T}_u = \frac{1}{2}m_U e\{\bar{V}^U\cdot\bar{V}^U\} \tag{21}
$$

The components of absolute velocity $\bar{V}^U$ of the unbalanced mass are given in the Appendix. Applying Lagrange's principle, the equations of motion of the unbalanced mass along the OY_b and OZ_b axes are obtained as given in

$$
\begin{aligned}
&- m_U e[\{(\dot{\Phi}+\Omega^b_{X_b})^2 + \Omega^{b^2}_{Z_b}\}\cos(\dot{\Phi}t+\gamma_U) \\
&\quad + (\ddot{\Phi}+\dot{\Omega}^b_{X_b} - \Omega^b_{Y_b}\Omega^b_{Z_b})\sin(\dot{\Phi}t+\gamma_U)] = 0 \\
&- m_U e[\{(\dot{\Phi}+\Omega^b_{X_b})^2 + \Omega^{b^2}_{Y_b}\}\sin(\dot{\Phi}t+\gamma_U) \\
&\quad - (\ddot{\Phi}+\dot{\Omega}^b_{X_b} + \Omega^b_{Y_b}\Omega^b_{Z_b})\cos(\dot{\Phi}t+\gamma_U)] = 0
\end{aligned}
\tag{22}
$$

E. Contribution of the Bearings

For nonflexible bearings, the displacement boundary conditions, given by Eq. (23), are imposed on the assembled finite element equation of the rotor-shaft-bearing system:

$$
v_{\text{brg}} = w_{\text{brg}} = 0 \tag{23}
$$

where the subscript brg stands for the displacement components of the shaft at the bearing node relative to the base.

The expression of force applied on the rotor due to the bearing flexibility is given as

$$
\{\boldsymbol{Q}\}_{\text{brg}} = -[\boldsymbol{D}]_{\text{brg}}\{\dot{\boldsymbol{q}}\} - [\boldsymbol{K}]_{\text{brg}}\{\boldsymbol{q}\} \tag{24}
$$

where $\{\boldsymbol{q}\}$ is the $n\times 1$ assembled global degrees-of-freedom vector for the rotor-shaft-bearing system, conforming to the connectivity of the finite elements, where n is the total number of degrees of freedom of the system, and $[\boldsymbol{D}]_{\text{brg}}$ and $[\boldsymbol{K}]_{\text{brg}}$ are two properly augmented sparse matrices, to take into account the damping and stiffness effects contributed by the bearings.

F. Assembled Equation for the Uncontrolled Rotor Shaft System

Equations of motion for the finite element model of the rotor-shaft-bearing system are obtained after appropriately assembling Eqs. (14), (20), and (22) for the individual discs and the shaft elements, as well as the mass unbalance as given in

$$
[\boldsymbol{M}]\{\ddot{\boldsymbol{q}}\} + [\boldsymbol{D}]\{\dot{\boldsymbol{q}}\} + [\boldsymbol{K}]\{\boldsymbol{q}\} = \{\boldsymbol{f}\} \tag{25}
$$

In the previous equation, $[\boldsymbol{M}]$ is the assembled inertia matrix, $[\boldsymbol{D}]$ is the assembled matrix (including the gyroscopic matrix, the matrix to account for the Coriolis component of the acceleration, the damping matrix, etc.) coefficient to the global velocity vector, and $[\boldsymbol{K}]$ is the assembled matrix (including the bending stiffness matrix, the circulatory matrix, the parametric stiffness matrices due to base motion, and the bearing stiffness matrix) coefficient to the global displacement vector. The global load vector $\{\boldsymbol{f}\}$ contains the effects of mass unbalance, inertia force due to base motion, and force due to gravity. It is to be noted that both the matrices $[\boldsymbol{K}]$ and $[\boldsymbol{D}]$ have time-dependent terms originating due to the base motion.

G. External Control Force from the Actuator and the Control Strategy

An electromagnetic actuator consisting of four electromagnetic exciters having two poles each, as shown in Fig. 3, is considered. For the arrangement of the electromagnets shown, it is possible to decouple the electromagnetic actuation force components along the Y and Z directions [26]. The actuator is placed on the stator, as shown in Fig. 1, at a suitable location along the span of the rotor, avoiding the disc and the bearing positions for convenience. Nighil et al. [19] has given details of obtaining the control force and proposed its use for controlling the steady synchronous rotor response under the sole influence of mass unbalance.

In short, following [19], the electromagnetic actuator may be modeled to have a stiffness of $(k_g k_i k_p - k_S)$ and a damping coefficient of $(k_g k_i k_v)$. The control force applied at the actuator node may be expressed as in Eq. (26); the corresponding expressions of the control currents [based on the proportional-plus-derivative (PD) control law applied to the displacement of the rotor section at the actuator node, as shown in the block diagram of Fig. 4) are given in Eq. (27):

$$
\begin{aligned}
F_Y &= -(k_g k_i k_p - k_S)v - k_g k_i k_v\dot{v} \\
F_Z &= -(k_g k_i k_p - k_S)w - k_g k_i k_v\dot{w}
\end{aligned}
\tag{26}
$$

$$
i_{cY} = -k_g\{k_p v + k_v\dot{v}\}; \qquad i_{cY} = -k_g\{k_p w + k_v\dot{w}\} \tag{27}
$$

In Eq. (26), k_i and k_S signify the force-current factor and force-displacement factor given by

$$
k_i = 4k_{\text{mag}}\frac{i_0}{g_0^2}; \qquad k_S = -4k_{\text{mag}}\frac{i_0^2}{g_0^3} \tag{28}
$$

where $k_{\text{mag}} = [(\mu_0 A_p N^2)/4]\cos(\alpha)$ is the magnetic exciter constant, in which A_p is the area of each pole face, N is the number of coil turns associated with a pair of poles, α is the semi-included angle between the adjacent poles (which is 22.5 deg for the setup shown in Fig. 3), and μ_0 is the magnetic permeability of the free air. The terms i_0 and g_0 denote the bias current in the exciter coils and the nominal air gap

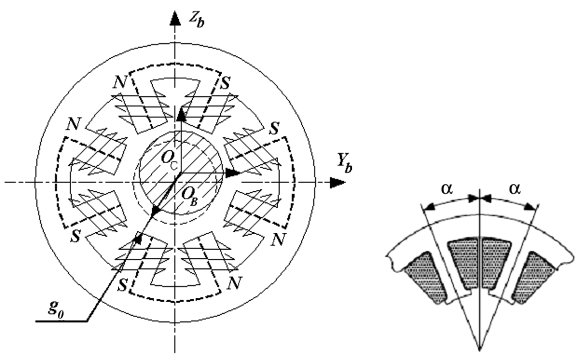

Fig. 3 Electromagnetic actuator a) stator configuration and b) arrangement of coils and poles.

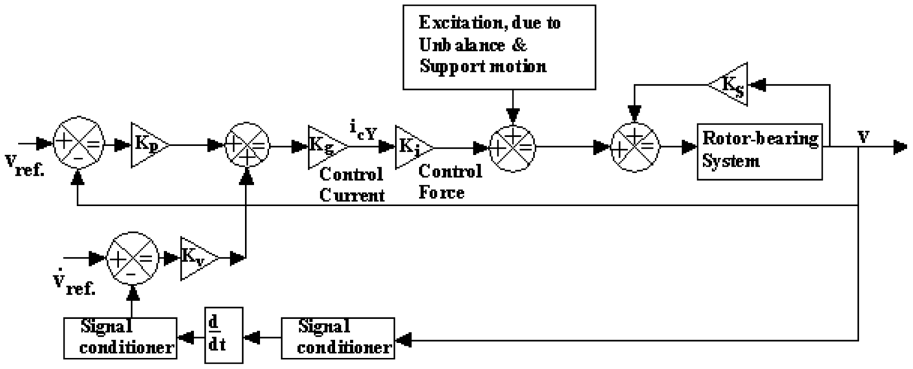

Fig. 4 Block diagram representation of the control strategy adopted by the electromagnetic actuator.

between the pole face and the rotor surface, respectively. In Eqs. (26) and (27) k_g, k_p, and k_v are the power amplifier gain (in A/V), the displacement feedback gain (V/m), and the velocity feedback gain (V · s/m), as shown schematically in Fig. 4.

In terms of the global degrees of freedom, the force applied by the actuator is written as in Eq. (29), in which $\{\boldsymbol{q}\}$ and $\{\dot{\boldsymbol{q}}\}$ are, respectively, the global displacement and velocity vectors, and $[K]_{\text{ac}}$ and $[D]_{\text{ac}}$ are two sparse matrices (the actuator stiffness and damping matrices, respectively) having nonzero stiffness and damping entries in rows and columns corresponding to the actuator node only:

$$\{\boldsymbol{Q}\}_C = -[\boldsymbol{K}]_{\text{ac}}\{\boldsymbol{q}\} - [\boldsymbol{D}]_{\text{ac}}\{\dot{\boldsymbol{q}}\} \tag{29}$$

Incorporating the expression of the control force from the actuator into the system equations of motion (25), the equations of motion of the controlled system are written as

$$[\boldsymbol{M}]\{\ddot{\boldsymbol{q}}\} + \{[\boldsymbol{D}] + [\boldsymbol{D}]_{\text{ac}}\}\{\dot{\boldsymbol{q}}\} + \{[\boldsymbol{K}] + [\boldsymbol{K}]_{\text{ac}}\}\{\boldsymbol{q}\} = \{\boldsymbol{f}\} \tag{30}$$

III. Results and Discussion

Numerical simulations are performed to show the effect of vehicle maneuver on rotor response and its attenuation by using the electromagnetic actuator. A similar rotor shaft system used by Duchemin et al. [15] is considered for this purpose, with the data shown in Table 1. It is supposed that the rotor is mounted on an aircraft, such that the rotor axis is parallel to that of the aircraft fuselage (i.e., the axis X_b of the frame F_b). The center of mass of the aircraft G, as well as the left support point of the rotor, which is the origin of the coordinate system (X_b–Y_b–Z_b), is located in the same (X_b–Y_b) plane, and the origin is located 10 m away to the left side and 5 m ahead of the aircraft center of mass (i.e., ${}_Gx^b = 5$ m, ${}_Gy^b = 10$ m, and ${}_Gz^b = 0$, as shown in Fig. 1). The bearings at the ends are considered rigid, and the presence of the mass unbalance is neglected to study the rotor motion due only to the inertia force generated by the aircraft motion. The rotor shaft system is discretized with four equal two-noded Rayleigh beam finite elements, with the disc being located at node 4 of the shaft. For the control action, the electromagnetic actuator is placed at node 3 (the midpoint of the shaft), and the parameters for the actuator and the control circuit are as follows: $N = 1000$, $A_p = 3$ cm^2, $g_0 = 2.5$ mm, $i_0 = 5$ A, $k_g = 0.8$ A/V, $k_p = 10$ V/m, and $k_v = 2$ V · s/m.

Table 1 Parameters of the rotor shaft system

Parameters	Values
Shaft length	0.4 m
Shaft radius	5 mm
Young's modulus of the shaft material	205.1 GPa
Density of both the shaft and the disc material	7800 kg/m^3
Disc radius	0.1 m
Disc thickness	10 mm
Location of the disc from the left end	0.3 m

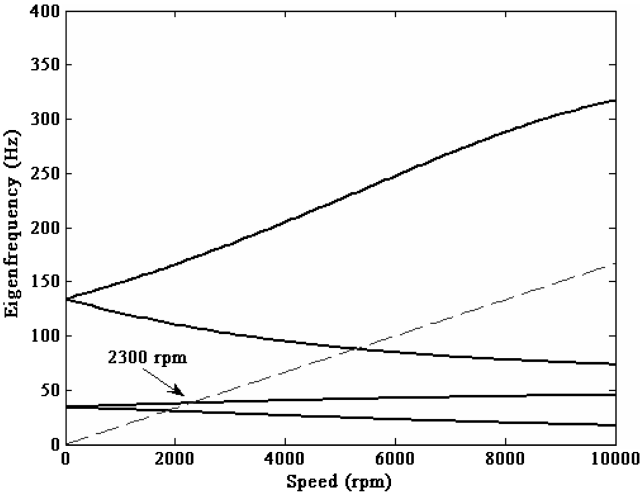

Fig. 5 Campbell diagram for the uncontrolled rotor-shaft-bearing system.

The Campbell diagram for the uncontrolled rotor, when the aircraft is either stationary or flying at a level with a constant velocity, is shown in Fig. 5. For this condition, critical speed of the rotor-shaft-bearing system is seen to be 2300 rpm.

Two different cases of maneuver are considered for the present study: case 1) a combined yawing and rolling motion, and case 2) a pitching motion. The motion in case 1 occurs when an aircraft negotiates a turn along a horizontal circular arc with a constant forward speed, causing the yawing motion, and at the same time rolls about the fuselage axis to provide the angle of banking. The motion in case 2 occurs when an aircraft dives in a vertical plane with a constant horizontal component of velocity.

A. Case 1

Let the aircraft negotiate a turn of radius of curvature of $\rho = 1800$ m with a constant forward speed V as its nose moves toward the right. The angle of banking during this maneuver is provided by the rolling of the aircraft about its axis, so that the left wing tip goes upward and the right wing tip goes downward. For a smooth flight, it is assumed that in the first phase (i.e., in the first 1 s), the aircraft turns as it rolls sinusoidally from $\gamma_R = 0$ deg to a maximum of $\gamma_R|_{\text{Max}}$ (which is chosen as equal to 20 deg or $\pi/9$ rad, unless otherwise stated), and in the next 1 s (the second phase), the aircraft rolls back (in the opposite sense) sinusoidally to achieve its initial horizontal configuration to continue flying at the same speed along the direction attained at the end of the first phase. The angle of roll γ_R and the roll rate $\dot{\gamma}_R$ are given by the following time functions:

$$\gamma_R(t) = (\gamma_R|_{\text{Max}}) \sin\left(\frac{\pi t}{2}\right) \tag{31a}$$

and

$$\dot{\gamma}_R(t) = \frac{\pi}{2}(\gamma_R|_{\text{Max}})\cos\left(\frac{\pi t}{2}\right) \tag{31b}$$

The yawing rate is given by

$$\dot{\beta}_Y = -\frac{V}{\rho} \tag{32}$$

The components of the velocity of the origin of F_b and the angular velocity components are given by Eqs. (33) and (34), respectively:

$$\left.\begin{aligned} V^b_{X_b} &= V + \dot{\beta}_Y\{{}_Gz^b\sin(\gamma_R) - {}_Gy^b\cos(\gamma_R)\} \\ V^b_{Y_b} &= \dot{\beta}_{YG}x^b\cos(\gamma_R) - \dot{\gamma}_{RG}z^b \\ V^b_{Z_b} &= -\dot{\beta}_{YG}x^b\sin(\gamma_R) + \dot{\gamma}_{RG}y^b \end{aligned}\right\} \tag{33}$$

$$\Omega^b_{X_b} = \dot{\gamma}_R; \qquad \Omega^b_{Y_b} = \dot{\beta}_Y\sin(\gamma_R); \qquad \Omega^b_{Z_b} = \dot{\beta}_Y\cos(\gamma_R) \tag{34}$$

Figure 6 shows the uncontrolled response components of the midpoint of the rotor shaft, relative to the base, over a time span of 4 s after the maneuver starts at $t = 0$ s and completes at $t = 2$ s, as the aircraft moves with a speed of $V = 200$ m/s (720 km/hr) and $\gamma_R|_{\text{Max}} = 20$ deg. The internal material damping is not considered in this case, as the rotor runs at 2000 rpm, which is well below the first critical speed indicated earlier. The resulting response amplitude is about 1 mm, and the individual components have contributions of harmonics of more than one frequency. Even after the maneuver stops after 2 s, the vibration does not die out owing to the lack of external damping in the system. The effect of the control action is visible from Fig. 7. With the same operating conditions, the controlled response amplitude is below 0.1 mm, thus yielding about a 90% reduction in the response. Also, the transient vibrations are quenched very quickly after the maneuver is complete.

Figures 8 and 9 show the effect of forward speed V on the uncontrolled and controlled rotor responses, respectively. For this purpose, simulation was performed for three different values of V (viz., 200, 80, and 320 m/s, respectively). A higher value of V increases the response amplitude, and a larger control force is required to achieve the same level of reduction.

Figure 10 shows the effect of maximum roll amplitude $\gamma_R|_{\text{Max}}$ on the controlled rotor response. Because the angle of rolling, and hence the rate of rolling, varies sinusoidally over time, increasing (or decreasing) $\gamma_R|_{\text{Max}}$ increases (or decreases) the roll rate at any instant of time. Three different values of $\gamma_R|_{\text{Max}}$ (namely 10, 20, and 25 deg) are chosen to study the effect of roll amplitude and the different roll rates on the controller performance shown by the ability of the controller to stabilize and attenuate the rotor response during maneuver. The largest value of $\gamma_R|_{\text{Max}}$ has been chosen to be 25 deg, keeping the passenger carriers in mind. It is observed that the higher the value

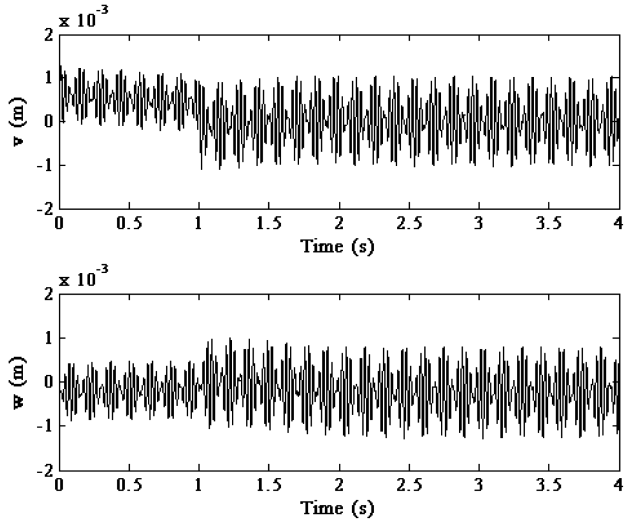

Fig. 6 Uncontrolled response during negotiation of a turn with the rotor spinning at 2000 rpm (without internal damping).

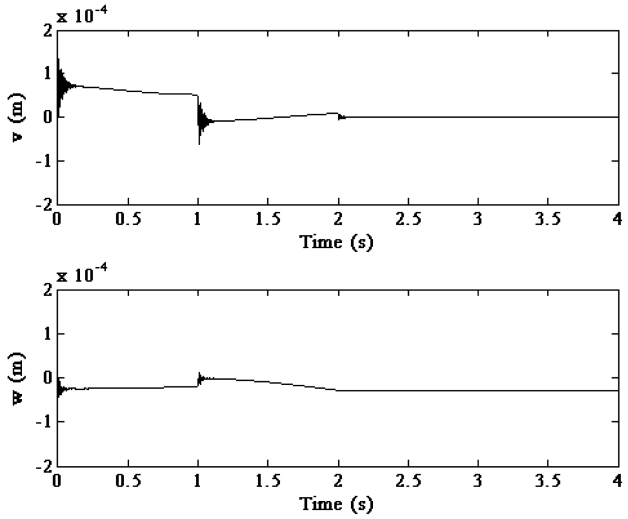

Fig. 7 Controlled response during negotiation of a turn with the rotor spinning at 2000 rpm (without internal damping).

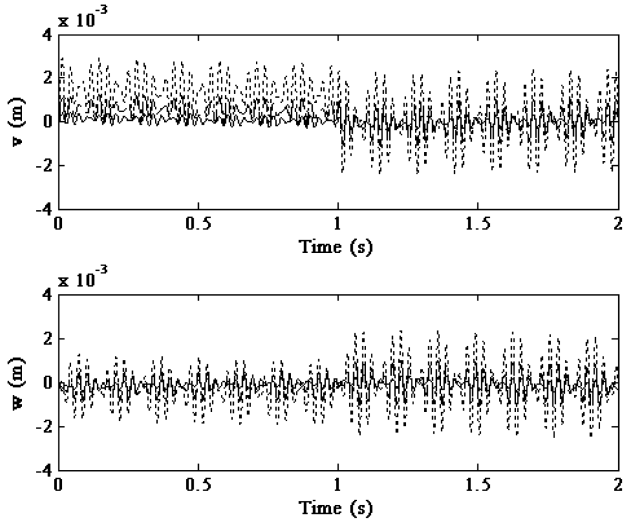

Fig. 8 Effect of aircraft forward speed on uncontrolled response during negotiation of a turn with the rotor spinning at 2000 rpm (without internal damping): $V = 200$ m/s (long-dashed line); $V = 80$ m/s (solid line); and $V = 320$ m/s (short-dashed line).

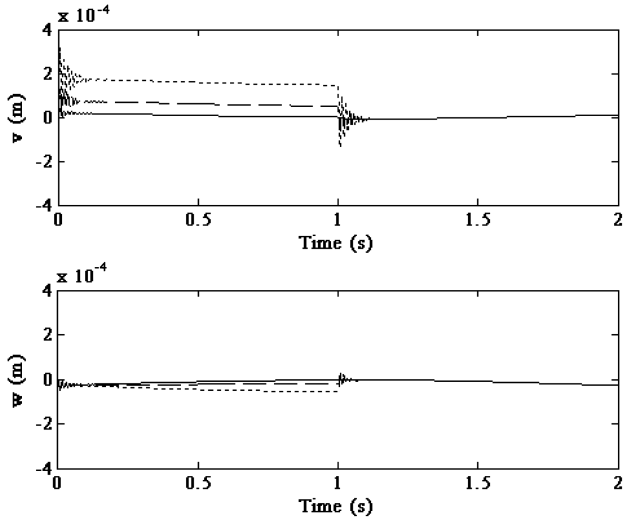

Fig. 9 Effect of aircraft forward speed on controlled response during negotiation of a turn with the rotor spinning at 2000 rpm (without internal damping): $V = 200$ m/s (long-dashed line); $V = 80$ m/s (solid line); and $V = 320$ m/s (short-dashed line).

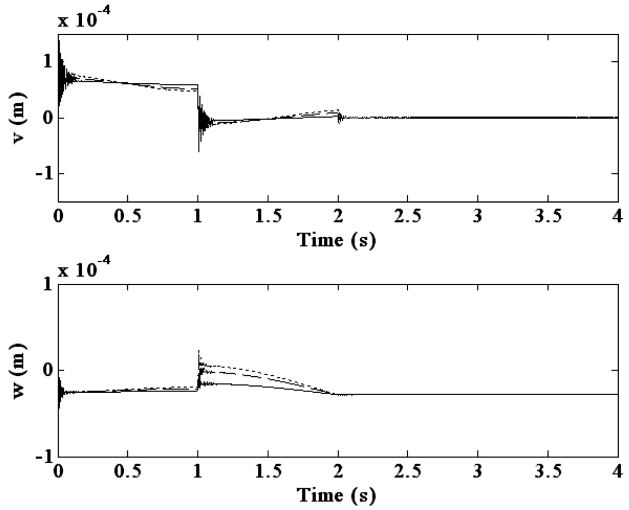

Fig. 10 Effect of roll amplitude of the aircraft on controlled response during negotiation of a turn with the rotor spinning at 2000 rpm (without internal damping): $\gamma_R|_{\text{Max}} = 10$ deg (solid line); $\gamma_R|_{\text{Max}} = 20$ deg (long-dashed line); and $\gamma_R|_{\text{Max}} = 25$ deg (short-dashed line).

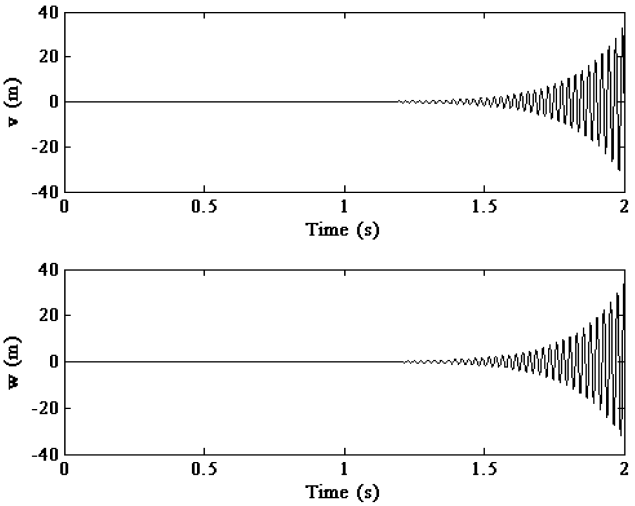

Fig. 11 Uncontrolled response during negotiation of a turn with the rotor spinning at 5000 rpm (with internal damping).

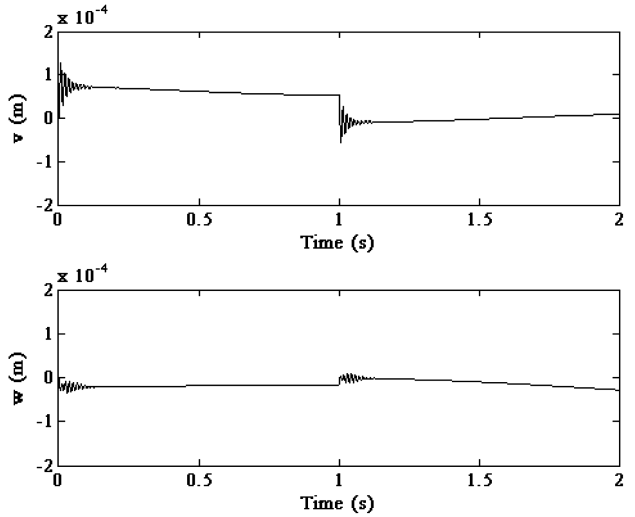

Fig. 12 Controlled response during negotiation of a turn with the rotor spinning at 5000 rpm (with internal damping).

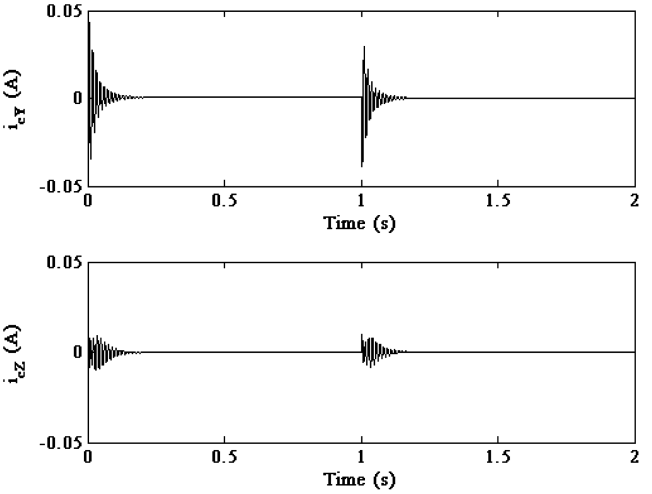

Fig. 13 Temporal variation of the control current during negotiation of a turn with the rotor spinning at 5000 rpm (with internal damping).

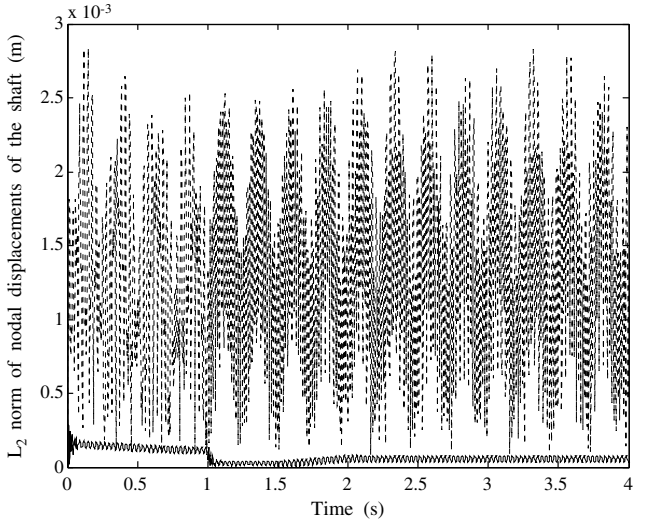

Fig. 14 Temporal variations of the L_2 norm of the nodal displacements of the rotor shaft system during negotiation of a turn, while the rotor is spinning at 2000 rpm, with mass unbalance at the disc (without internal damping): uncontrolled system (dashed line); and controlled system (solid line).

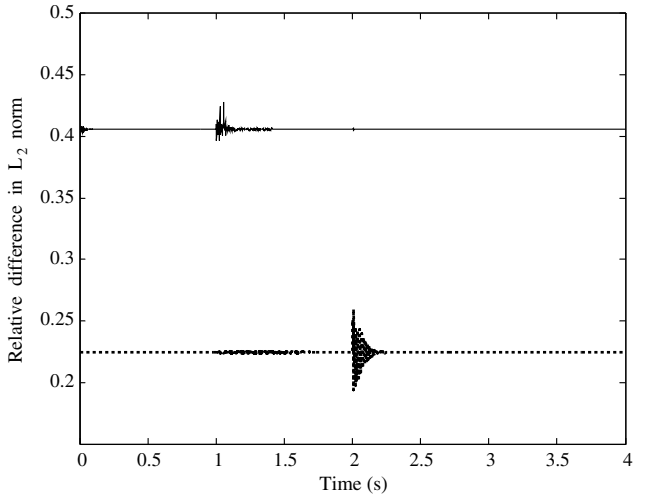

Fig. 15 Temporal variations of the relative difference of the L_2 norm of the nodal displacements of the controlled rotor-bearing system during negotiation of a turn, while the rotor is spinning at 2000 rpm (without internal damping): ${}_4e_8$ (solid line); and ${}_8e_{12}$ (dashed line).

of $\gamma_R|_{\text{Max}}$, the higher the transient response; however, the increment is marginal, and the controlled response settles down to the steady state (the settling time being the same, irrespective of the value of $\gamma_R|_{\text{Max}}$). So that the controller is found to be quite efficient in controlling the transient vibrations due to the different roll rates and roll amplitudes. However, the controller applies a larger force of actuation, needed to achieve the same level of reduction for a larger $\gamma_R|_{\text{Max}}$; this is the advantage of having an active controller.

Figures 11 and 12 show the uncontrolled and controlled response components of the midpoint of the shaft when the rotor spins at 5000 rpm and the aircraft moves at a speed of 200 m/s. Because the spin speed is above critical, the role of the internal material damping of the shaft becomes important. It is seen from Fig. 11 that the response components increase monotonically and indefinitely with time. In this case, the coefficient of the viscous form of internal damping is considered as $\eta_v = 0.0002$ s (after [25]). With the introduction of control action (as seen in Fig. 12), the response components are not only stabilized well, but the amplitude is reduced below 0.1 mm also. This achievement is due to two facts: 1) the stiffness effect employed through the control action increases the critical speed of the system and postpones the threshold of instability; and 2) the external stationary damping provided by the actuator limits the response further. The cost of control in terms of the control current components (i_{cY} and i_{cZ}) are shown in Fig. 13. The control action and the use of linearized control force about the operating point are justified, as the maximum control current is less than 0.05 A (1% of the bias current i_0).

Figure 14 shows the time variation of the Euclidean norm (L_2 norm) of the nodal displacements of the rotor shaft system undergoing vibration by inertial and parametric excitation caused by the vehicle maneuver, as well as the unbalanced excitation generated by the rotor spin. The disc is assumed to have a mass unbalance of 0.2×10^{-3} kg · m. As expected, there is a noticeable decrease in the level of the L_2 norm when the control force is applied. It is also observed that, due to the presence of unbalanced excitation in addition to inertial as well as parametric excitations, there is a persistent oscillation after the system has reached the steady state, but the level of such vibration amplitude under the control action is much less when compared with that of an uncontrolled rotor.

Figure 15 shows the comparison of the temporal variation of the relative difference in the L_2 norm of the nodal displacements for the controlled rotor-bearing system by increasing in steps the number of elements (from 4 to 8, and then from 8 to 12 elements) to discretize the rotor shaft continuum. This figure is plotted to investigate the possibility of a spillover of control energy into the unmodeled modes, a problem that may appear whenever an attempt is made to control a continuous system (truly having infinite degrees of freedom) with the help of a finite number of actuators working on the feedback signal measured by a finite number of sensors. The number of elements is increased in steps to include a few higher modes (previously unaccounted for when fewer elements are used) in the model and, in this process, get an idea about the possibility of spillover from the relative difference in the L_2 norm. The relative difference in the L_2 norm denoted by ${}_ie_j$ and is defined as follows:

$$ {}_ie_j = \frac{L_2 \text{ norm with } j \text{ no. of finite elements } - L_2 \text{ norm with } i \text{ no. of finite elements}}{L_2 \text{ norm with } i \text{ no. of finite elements}} $$

For example, with 12 finite elements, the number of pairs of complex conjugate vibration modes included in the model is 48, as opposed to 16 if four elements are used. It is observed from Fig. 15 that ${}_8e_{12} < {}_4e_8$. Noting that the L_2 norm computed over the shaft nodal displacements serves as an indicator of energy content of the vibrating rotor shaft, Fig. 15 signifies that it becomes increasingly difficult to excite the higher modes or, in other words, the higher modes have a lesser influence on determining the actual vibration

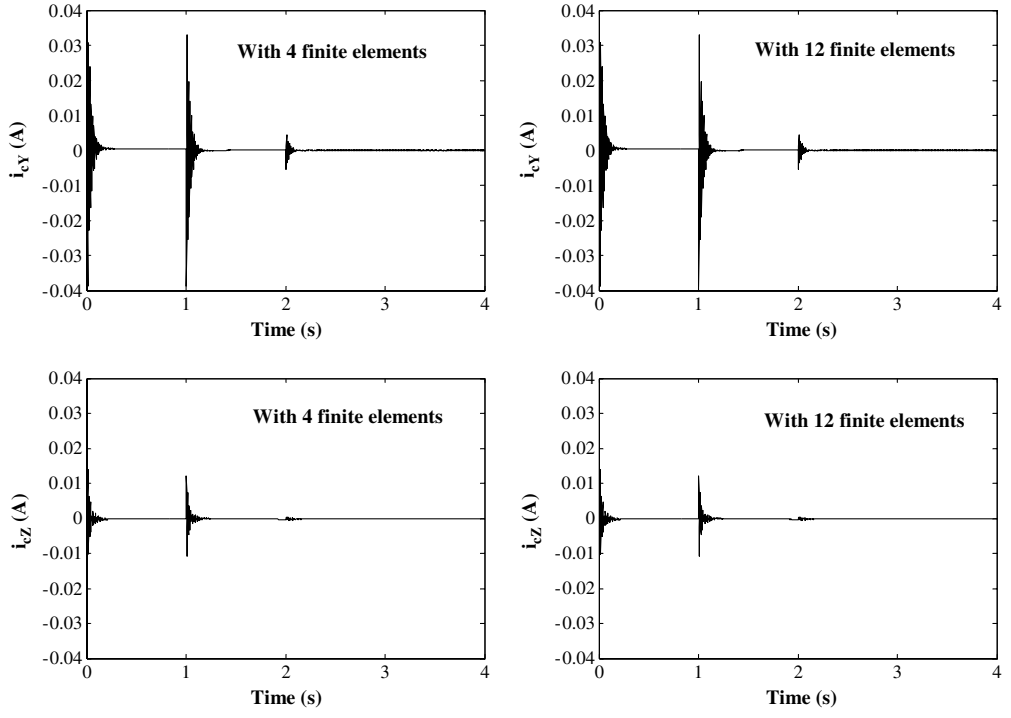

Fig. 16 Comparison of the temporal variation of the control current during the negotiation of a turn while the rotor is spinning at 2000 rpm (without internal damping).

levels. This results in a fall of the relative difference in the L_2 norm as the number of elements is increased. The comparison of the relative L_2 norm thus proves that there is hardly any possibility of spillover in this case. A similar conclusion was also drawn by Meirovitch and Baruh [27]. For the present problem, a good amount of external damping is applied on the vibrating rotor shaft system through the electromagnetic actuator, using the PD control strategy. Therefore, in practice, damping will be much larger for higher (unmodeled) modes than lower ones, and so the higher modes are not likely to be excited easily.

As a further check, the control current (which also depicts the amount of control effort spent) is plotted in Fig. 16, for which 4 and 12 elements are used to discretize the rotor continuum. A comparison of control currents shows hardly any difference as the number of elements is increased.

Therefore, a check of the relative difference in the L_2 norm and the control current with an increased number of elements may be followed as a guideline to check the robustness of the controller under general conditions.

B. Case 2

The aircraft is considered to dive in a vertical plane through a height H along a path approximated by a negative half of a sine curve defined by the coordinate of the aircraft center of mass along the OZ_0 axis (z_0^G). Equation (35) defines the path as a function of time t:

$$z_0^G(t) = H \sin\left(\frac{2\pi V_{X_0}^G t}{\lambda}\right) \tag{35}$$

where the constant horizontal velocity component ($V_{X_0}^G$) of the center of mass of the aircraft is assumed to be 200 m/s, and $\lambda = 850$ m is twice the length of the path over which the aircraft dives. The total duration of the maneuver is assumed to be $t = 2$ s. During this maneuver, no rolling, yawing, or side slipping takes place. The angle of pitching α_P is defined by following time functions:

$$\tan\alpha_P = \frac{V_{Z_0}^G}{V_{X_0}^G} = \frac{2\pi H}{\lambda}\cos\left(\frac{2\pi V_{X_0}^G t}{\lambda}\right) \tag{36}$$

The components of the velocity of the origin of F_b are given by

$$\left.\begin{aligned} V_{X_b}^b &= V_{X_0}^G \sec(\alpha_P) + {}_G z^b \dot{\alpha}_P \\ V_{X_b}^b &= 0 \\ V_{X_b}^b &= -{}_G x^b \dot{\alpha}_P \end{aligned}\right\} \tag{37}$$

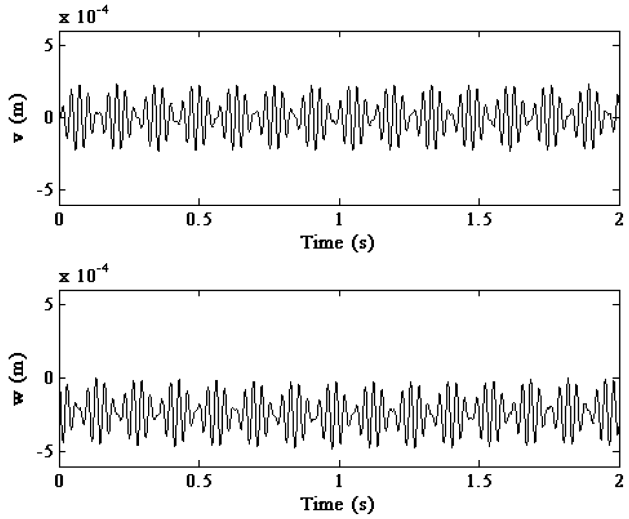

Fig. 17 Uncontrolled response during diving in a sine curve with the rotor spinning at 2000 rpm (without internal damping).

$$\Omega_{X_b}^b = 0; \qquad \Omega_{Y_b}^b = \dot{\alpha}_P; \qquad \Omega_{Z_b}^b = 0 \tag{38}$$

Figure 17 shows the uncontrolled response components of the rotor at its midpoint, over 2 s when the rotor spins at 2000 rpm, and the depth of dive H is taken as 50 m. The uncontrolled response has different harmonic components, as in the previous case, and the response amplitude is about 0.5 mm. The effect of control is obvious from Fig. 18. The transient part of the vibration diminishes very fast, and the response amplitude becomes negligibly small along the Y_b direction and ≤ 0.05 mm along the Z_b direction. The nonzero response along the Z_b direction is due to the static weight of the rotor.

Figures 19 and 20 show the uncontrolled and controlled response components, respectively, for different values of H. With an increase in H, the uncontrolled response apparently decreases, but in the case of controlled response, the sag along the vertical direction reaches a maximum when the aircraft is at the lowest point of its course, and then again decreases to the residual sag. The maximum sag is higher for higher values of H, but the residual sag is more for lower H. However, for controlled response, this sag is negligible ($\sim$10%) when compared with the uncontrolled response amplitude ($\approx$0.5 mm), and this justifies the control action.

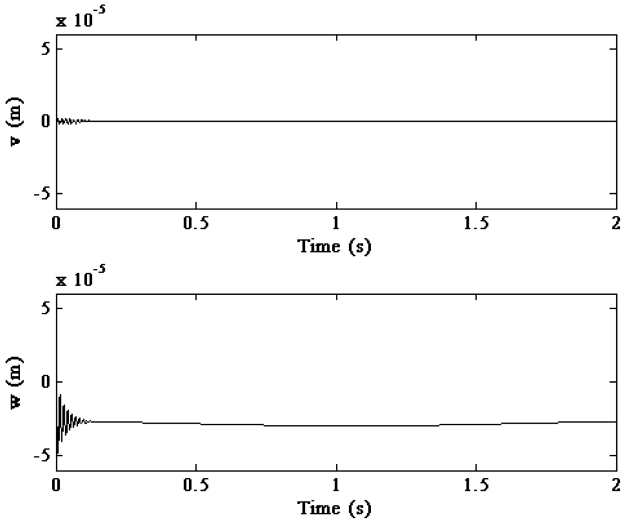

Fig. 18 Controlled response during diving in a sine curve with the rotor spinning at 2000 rpm (without internal damping).

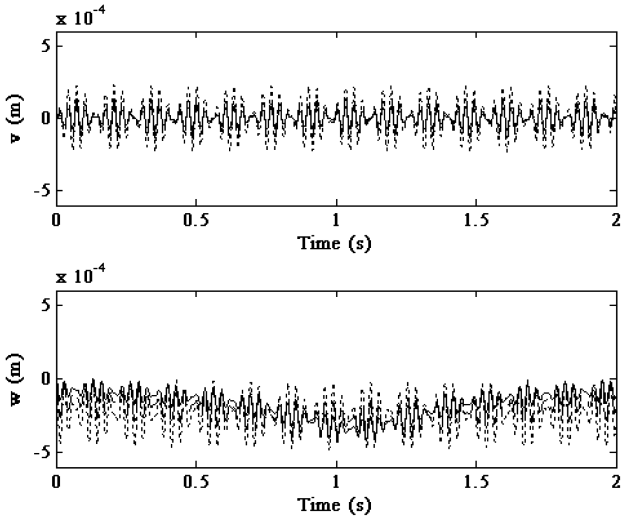

Fig. 19 Effect of the depth of dive on the uncontrolled response during diving in a sine curve with the rotor spinning at 2000 rpm (without internal damping): $H = 50$ m (short-dashed line); $H = 200$ m (long-dashed line); and $H = 400$ m (solid line).

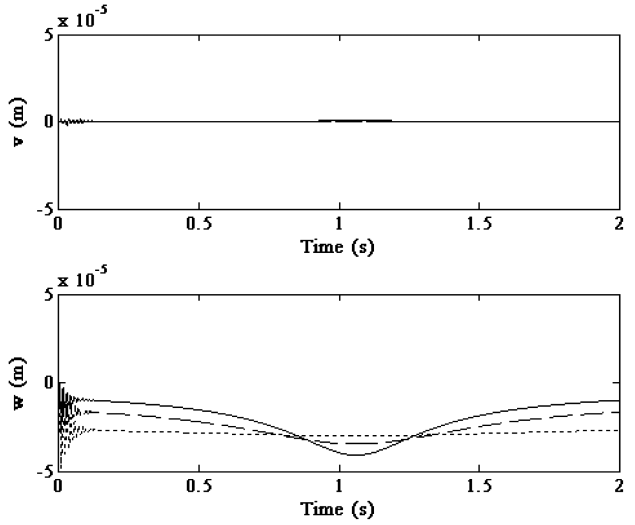

Fig. 20 Effect of the depth of dive on the controlled response during diving in a sine curve with the rotor spinning at 2000 rpm (without internal damping): $H = 50$ m (short-dashed line); $H = 200$ m (long-dashed line); and $H = 400$ m (solid line).

IV. Conclusions

From the previous discussions, it may be concluded that:

1) A flexible rotor shaft system is subjected to considerable transverse vibration under the effect of inertia force due to vehicle maneuvers like rolling, pitching, yawing, or any combination thereof, and one electromagnetic actuator with the PD control strategy on the rotor displacement at the actuator location is found very efficient to improve stability and to control the resulting rotor vibrations.

2) In a maneuvering aircraft, the transverse rotor response increases with the aircraft speed during both turning and diving, and with the maximum depth of diving. The controller is efficient enough to control the rotor vibration after the maneuver stops.

3) The controller enables the rotor operation in the supercritical speed regime, with respect to the uncontrolled situation of the rotor, by improving the stability limit of the spin speed of the rotor shaft system due to the internal material damping of the rotor shaft.

4) The relative difference in the L_2 norm and the control current may be checked with the increased number of elements as a guideline to test the possibility of a spillover and also the robustness of the controller under general conditions. Decreasing values of the relative difference in the L_2 norm, as well as the unchanged control current, signify the absence of spillover.

Appendix: Angular Velocity Components of the Frame F_s and Different Matrices

Components of angular velocity of the frame F_S:

$$\omega_{X_S} = (\dot{\Phi} - \dot{\Gamma}\sin \mathrm{B}) + \Omega^b_{X_b}\cos\Gamma\cos \mathrm{B} + \Omega^b_{Y_b}\sin\Gamma\cos \mathrm{B} - \Omega^b_{Z_b}\sin \mathrm{B}$$

$$\omega_{Y_S} = (\dot{\Gamma}\cos \mathrm{B}\sin\Phi + \dot{\mathrm{B}}\cos\Phi) + \Omega^b_{X_b}(\cos\Gamma\sin \mathrm{B}\sin\Phi - \sin\Gamma\cos\Phi) + \Omega^b_{Y_b}(\sin\Gamma\sin \mathrm{B}\sin\Phi + \cos\Gamma\cos\Phi) + \Omega^b_{Z_b}\cos \mathrm{B}\sin\Phi$$

$$\omega_{Z_S} = (\dot{\Gamma}\cos \mathrm{B}\cos\Phi - \dot{\mathrm{B}}\sin\Phi) + \Omega^b_{X_b}(\cos\Gamma\sin \mathrm{B}\cos\Phi + \sin\Gamma\sin\Phi) + \Omega^b_{Y_b}(\sin\Gamma\sin \mathrm{B}\cos\Phi - \cos\Gamma\sin\Phi) + \Omega^b_{Z_b}\cos \mathrm{B}\cos\Phi$$

Shape functions for the Rayleigh beam finite element:

$$\psi_1 = 1 - 3\left(\frac{x}{l}\right)^2 + 2\left(\frac{x}{l}\right)^3; \quad \psi_2 = l\left[\left(\frac{x}{l}\right) - 2\left(\frac{x}{l}\right)^2 + \left(\frac{x}{l}\right)^3\right]$$

$$\psi_3 = 3\left(\frac{x}{l}\right)^2 - 2\left(\frac{x}{l}\right)^3; \quad \psi_4 = l\left[-\left(\frac{x}{l}\right)^2 + \left(\frac{x}{l}\right)^3\right]$$

The shape function matrix:

$$[\Psi(x)] = \begin{bmatrix} \psi_1 & 0 & 0 & \psi_2 & \psi_3 & 0 & 0 & \psi_4 \\ 0 & \psi_1 & -\psi_2 & 0 & 0 & \psi_3 & -\psi_4 & 0 \end{bmatrix}$$

Different matrices for a shaft finite element:

Inertia matrix:

$$[\boldsymbol{M}]^e_S = [\boldsymbol{M}_T]^e_S + [\boldsymbol{M}_R]^e_S = \int_0^l m[\Psi]^T[\Psi]\,\mathrm{d}x + \int_0^l i_d[\Psi']^T[\Psi']\,\mathrm{d}x$$

Gyroscopic matrix:

$$[\boldsymbol{G}]^e_S = [\boldsymbol{H}]^e_S - [\boldsymbol{H}]^{e^T}_S = \int_0^l i_p[\psi']^T\begin{bmatrix} 0 & -1 \\ 1 & 0 \end{bmatrix}[\psi']\,\mathrm{d}x$$

and the matrix

$$[\boldsymbol{H}]^e_S = \int_0^l i_p[\psi']^T\begin{bmatrix} 0 & 0 \\ 1 & 0 \end{bmatrix}[\psi']\,\mathrm{d}x$$

Matrix to account for the Coriolis component of the acceleration:

$$[\boldsymbol{C}]^e_S = [\boldsymbol{C}_T]^e_S + [\boldsymbol{C}_R]^e_S = \int_0^l m[\Psi]^T\begin{bmatrix} 0 & -1 \\ 1 & 0 \end{bmatrix}[\Psi]\,\mathrm{d}x + \int_0^l i_d[\Psi']^T\begin{bmatrix} 0 & -1 \\ 1 & 0 \end{bmatrix}[\Psi']\,\mathrm{d}x$$

Bending stiffness matrix:

$$[\boldsymbol{K}_B]^e_S = \int_0^l EI[\Psi'']^T[\Psi'']\,\mathrm{d}x$$

Circulatory matrix:

$$[\boldsymbol{K}_C]^e_S = \int_0^l EI[\Psi'']^T\begin{bmatrix} 0 & 1 \\ -1 & 0 \end{bmatrix}[\Psi'']\,\mathrm{d}x$$

Parametric stiffness matrices due to base rotation:

$$[\boldsymbol{K}_{p11}]^e_S = \int_0^l m[\Psi]^T\begin{bmatrix} 1 & 0 \\ 0 & 0 \end{bmatrix}[\Psi]\,\mathrm{d}x + \int_0^l i_p[\Psi']^T\begin{bmatrix} 0 & 0 \\ 0 & 1 \end{bmatrix}[\Psi']\,\mathrm{d}x$$

$$[\boldsymbol{K}_{p22}]^e_S = \int_0^l m[\Psi]^T\begin{bmatrix} 0 & 0 \\ 0 & 1 \end{bmatrix}[\Psi]\,\mathrm{d}x + \int_0^l i_p[\Psi']^T\begin{bmatrix} 1 & 0 \\ 0 & 0 \end{bmatrix}[\Psi']\,\mathrm{d}x$$

$$[\boldsymbol{K}_{p12}]^e_S = \int_0^l m[\Psi]^T\begin{bmatrix} 0 & 1 \\ 1 & 0 \end{bmatrix}[\Psi]\,\mathrm{d}x + \int_0^l i_p[\Psi']^T\begin{bmatrix} 0 & 1 \\ 1 & 0 \end{bmatrix}[\Psi']\,\mathrm{d}x$$

Load vectors:

$$\{\boldsymbol{S}_{2Y}\}^e_S = \int_0^l mx[\Psi(x)]^T\begin{Bmatrix} 1 \\ 0 \end{Bmatrix}\mathrm{d}x + \int_0^l i_d[\Psi'(x)]^T\begin{Bmatrix} 0 \\ 1 \end{Bmatrix}\mathrm{d}x$$

$$\{\boldsymbol{S}_{2P}\}^e_S = \int_0^l mx[\Psi(x)]^T\begin{Bmatrix} 0 \\ 1 \end{Bmatrix}\mathrm{d}x - \int_0^l i_d[\Psi'(x)]^T\begin{Bmatrix} 1 \\ 0 \end{Bmatrix}\mathrm{d}x$$

$$\{\boldsymbol{S}_{1Y}\}^e_S = \int_0^l i_p[\Psi'(x)]^T\begin{Bmatrix} 1 \\ 0 \end{Bmatrix}\mathrm{d}x; \quad \{\boldsymbol{S}_{1P}\}^e_S = \int_0^l i_p[\Psi'(x)]^T\begin{Bmatrix} 0 \\ 1 \end{Bmatrix}\mathrm{d}x$$

$$\{\boldsymbol{S}_1\}^e_S = \int_0^l m[\Psi(x)]^T\begin{Bmatrix} 1 \\ 0 \end{Bmatrix}\mathrm{d}x; \quad \{\boldsymbol{S}_2\}^e_S = \int_0^l m[\Psi(x)]^T\begin{Bmatrix} 0 \\ 1 \end{Bmatrix}\mathrm{d}x$$

Different matrices for a disc:
Inertia matrix:

$$[\boldsymbol{M}]_D = \begin{bmatrix} m_D & 0 & 0 & 0 \\ 0 & m_D & 0 & 0 \\ 0 & 0 & I_d & 0 \\ 0 & 0 & 0 & I_d \end{bmatrix}$$

Gyroscopic matrix:

$$[\boldsymbol{G}]_D = [\boldsymbol{H}]_D - [\boldsymbol{H}]_D^T = \begin{bmatrix} 0 & 0 & 0 & 0 \\ 0 & 0 & 0 & 0 \\ 0 & 0 & 0 & -I_p \\ 0 & 0 & I_p & 0 \end{bmatrix}$$

Matrix to account for the Coriolis component of the acceleration:

$$[\boldsymbol{C}]_D = \begin{bmatrix} 0 & -m_D & 0 & 0 \\ m_D & 0 & 0 & 0 \\ 0 & 0 & 0 & -I_d \\ 0 & 0 & I_d & 0 \end{bmatrix}$$

Parametric stiffness matrices:

$$[\boldsymbol{K}_{p11}]_D = \begin{bmatrix} m_D & 0 & 0 & 0 \\ 0 & 0 & 0 & 0 \\ 0 & 0 & I_p & 0 \\ 0 & 0 & 0 & 0 \end{bmatrix}$$

$$[\boldsymbol{K}_{p22}]_D = \begin{bmatrix} 0 & 0 & 0 & 0 \\ 0 & m_D & 0 & 0 \\ 0 & 0 & 0 & 0 \\ 0 & 0 & 0 & I_p \end{bmatrix}$$

$$[\boldsymbol{K}_{p12}]_D = \begin{bmatrix} 0 & m_D & 0 & 0 \\ m_D & 0 & 0 & 0 \\ 0 & 0 & 0 & I_p - I_d \\ 0 & 0 & I_p - I_d & 0 \end{bmatrix}$$

Load vectors:

$$\{\boldsymbol{S}_{2Y}\}_D = [\, m_D x_D \quad 0 \quad 0 \quad I_d \,]^T$$
$$\{\boldsymbol{S}_{2P}\}_D = [\, 0 \quad m_D x_D \quad -I_d \quad 0 \,]^T$$
$$\{\boldsymbol{S}_{1Y}\}_D = [\, 0 \quad 0 \quad 0 \quad I_p \,]^T; \qquad \{\boldsymbol{S}_{1P}\}_D = [\, 0 \quad 0 \quad I_p \quad 0 \,]^T$$
$$\{\boldsymbol{S}_1\}_D = [\, m_D \quad 0 \quad 0 \quad 0 \,]^T; \qquad \{\boldsymbol{S}_2\}_D = [\, 0 \quad m_D \quad 0 \quad 0 \,]^T$$

Mass unbalance matrix associated with a disc:

$$[UB] = \begin{bmatrix} m_U e & 0 \\ 0 & m_U e \\ 0 & 0 \\ 0 & 0 \end{bmatrix}$$

Velocity of the unbalance mass:

$$\bar{V}^U = \begin{Bmatrix} V_{X_b}^b + \Omega_{Y_b}^b \{w_D + e\sin(\dot{\Phi}t + \gamma_U)\} - \Omega_{Z_b}^b \{v_D + e\cos(\dot{\Phi}t + \gamma_U)\} \\ V_{Y_b}^b + \Omega_{Z_b}^b x_D - \Omega_{X_b}^b \{w_D + e\sin(\dot{\Phi}t + \gamma_U)\} + \dot{v}_D - \dot{\Phi} e\sin(\dot{\Phi}t + \gamma_U) \\ V_{Z_b}^b - \Omega_{Y_b}^b x_D + \Omega_{X_b}^b \{v_D + e\cos(\dot{\Phi}t + \gamma_U)\} + \dot{w}_D + \dot{\Phi} e\cos(\dot{\Phi}t + \gamma_U) \end{Bmatrix}$$

Global matrices and vectors:

$$[\boldsymbol{M}] = \sum_D [\boldsymbol{M}]_D + \sum_e [\boldsymbol{M}]_S^e$$

$$[\boldsymbol{D}] = -(\dot{\Phi} + \Omega_{X_b}^b)\left(\sum_D [\boldsymbol{G}]_D + \sum_e [\boldsymbol{G}]_S^e\right) + 2\Omega_{X_b}^b \left(\sum_D [\boldsymbol{C}]_D + \sum_e [\boldsymbol{C}]_S^e\right) + \eta_v \sum_e [\boldsymbol{K}_B]_S^e + [\boldsymbol{D}]_{\text{brg}}$$

$$[\boldsymbol{K}] = \sum_e [\boldsymbol{K}_B]_S^e + \eta_v \dot{\Phi} \sum_e [\boldsymbol{K}_C]_S^e + [\boldsymbol{K}]_{\text{brg}} + \dot{\Omega}_{X_b}^b \left(\sum_D [\boldsymbol{C}]_D + \sum_e [\boldsymbol{C}]_S^e\right) - \Omega_{X_b}^{b^2} \left(\sum_D [\boldsymbol{M}]_D + \sum_e [\boldsymbol{M}]_S^e\right) - (\ddot{\Phi} + \dot{\Omega}_{X_b}^b)\left(\sum_D [\boldsymbol{H}]_D + \sum_e [\boldsymbol{H}]_S^e\right) - \Omega_{Z_b}^{b^2} \left(\sum_D [\boldsymbol{K}_{p11}]_D + \sum_e [\boldsymbol{K}_{p11}]_S^e\right) - \Omega_{Y_b}^{b^2} \left(\sum_D [\boldsymbol{K}_{p22}]_D + \sum_e [\boldsymbol{K}_{p22}]_S^e\right) - \Omega_{Y_b}^b \Omega_{Z_b}^b \left(\sum_D [\boldsymbol{K}_{p12}]_D + \sum_e [\boldsymbol{K}_{p12}]_S^e\right)$$

$$\{f\} = \sum_D [UB] \begin{Bmatrix} [(\dot{\Phi} + \Omega_{X_b}^b)^2 + \Omega_{Z_b}^{b2}]\cos(\Phi + \gamma_U) \\ +(\ddot{\Phi} + \dot{\Omega}_{X_b}^b - \Omega_{Y_b}^b \Omega_{Z_b}^b)\sin(\Phi + \gamma_U) \\ [(\dot{\Phi} + \Omega_{X_b}^b)^2 + \Omega_{Y_b}^{b2}]\sin(\Phi + \gamma_U) \\ -(\ddot{\Phi} + \dot{\Omega}_{X_b}^b + \Omega_{Y_b}^b \Omega_{Z_b}^b)\cos(\Phi + \gamma_U) \end{Bmatrix} - (\dot{\Omega}_{Z_b}^b + \Omega_{X_b}^b \Omega_{Y_b}^b)\left(\sum_D \{\boldsymbol{S}_{2Y}\}_D + \sum_e \{\boldsymbol{S}_{2Y}\}_S^e\right) + (\dot{\Omega}_{Y_b}^b + \Omega_{X_b}^b \Omega_{Z_b}^b)\left(\sum_D \{\boldsymbol{S}_{2P}\}_D + \sum_e \{\boldsymbol{S}_{2P}\}_S^e\right) - (\dot{\Phi} + \Omega_{X_b}^b)\Omega_{Z_b}^b \left[\sum_D \{\boldsymbol{S}_{1P}\}_D + \sum_e \{\boldsymbol{S}_{1P}\}_S^e\right] + (\dot{\Phi} + \Omega_{X_b}^b)\Omega_{Y_b}^b \left[\sum_D \{\boldsymbol{S}_{1Y}\}_D + \sum_e \{\boldsymbol{S}_{1Y}\}_S^e\right] - (\dot{V}_{Y_b}^b + V_{X_b}^b \Omega_{Z_b}^b - V_{Z_b}^b \Omega_{X_b}^b)\left(\sum_D \{\boldsymbol{S}_1\}_D + \sum_e \{\boldsymbol{S}_1\}_S^e\right) - (\dot{V}_{Z_b}^b - V_{X_b}^b \Omega_{Y_b}^b - V_{Y_b}^b \Omega_{X_b}^b)\left(\sum_D \{\boldsymbol{S}_2\}_D + \sum_e \{\boldsymbol{S}_2\}_S^e\right) - g(\cos\alpha_P \sin\gamma_R + \sin\alpha_P \sin\beta_Y \cos\gamma_R) \times \left(\sum_D \{\boldsymbol{S}_1\}_D + \sum_e \{\boldsymbol{S}_1\}_S^e\right) - g(\cos\alpha_P \cos\gamma_R - \sin\alpha_P \sin\beta_Y \sin\gamma_R)\left(\sum_D \{\boldsymbol{S}_1\}_D + \sum_e \{\boldsymbol{S}_1\}_S^e\right)$$

The symbol $\sum$ stands for the assembly of finite element matrices and vectors after the appropriate globalization method is followed.

Acknowledgments

The short-term support from the German Academic Exchange Service (DAAD) is gratefully acknowledged. J.K. Dutt expresses his gratitude to H. Irretier of the Institute of Mechanics at the University

of Kassel for initiating a research work on the concept of active vibration control of rotors with a single actuator during his visit to the University of Kassel to work with H. Irretier on a short-term fellowship from DAAD from November 2003 to January 2004.

References

[1] Tessarzik, J. M., Chiang, T., and Badgley, R. H., "The Response of Rotating Machinery to External Random Vibration," *Journal of Engineering for Industry*, Vol. 96, No. 2, 1974, pp. 477–489.

[2] Nakamura, K., Fukui, S., and Oowa, T., "Aseismic Design of Uranium Centrifuges," *Journal of the Japan Society of Mechanical Engineers*, Vol. 79, No. 689, 1976, pp. 92–95.

[3] Iwatsubo, T., Kawahara, I., Nakagawa, N., and Kawai, R., "Reliability Design of Rotating Machine Against Earthquake Excitation," *Bulletin of the JSME*, Vol. 22, No. 173, 1979, pp. 1632–1639.

[4] Lund, J. W., "Response Characteristics of a Rotor with Flexible Damped Supports," *Symposium Dynamics of Rotors, IUTAM Lyngby*, Springer–Verlag, Berlin, 1975, pp. 319–349.

[5] Soni, A. H., and Srinivasan, V., "Seismic Analysis of a Gyroscopic Mechanical System," *Journal of Vibration, Acoustics, Stress, and Reliability in Design*, Vol. 105, No. 2, 1983, pp. 449–455.

[6] Srinivasan, V., and Soni, A. H., "Seismic Analysis of a Rotor-Bearing System," *Earthquake Engineering and Structural Dynamics*, Vol. 12, No. 3, 1984, pp. 287–311.
doi:10.1002/eqe.4290120302

[7] Subbiah, R., Bhat, R. B., and Sankar, T. S., "Response of Rotors Subjected to Random Support Excitation," *Journal of Vibration, Acoustics, Stress, and Reliability in Design*, Vol. 107, No. 4, 1985, pp. 453–461.

[8] Samali, B., Kim, K. B., and Yang, J. N., "Random Vibration of Rotating Machines Under Earthquake Excitation," *ASCE: Journal of Engineering Mechanics*, Vol. 112, No. 6, 1986, pp. 550–565.
doi:10.1061/(ASCE)0733-9399(1986)112:6(550)

[9] Singh, M. P., Chang, T. S., and Suarez, L. E., "A Response Spectrum Method for Seismic Design Evaluation of Rotating Machines," *Journal of Vibration and Acoustics*, Vol. 114, No. 4, 1992, pp. 454–460.
doi:10.1115/1.2930284

[10] Su, W. C., Hernreid, A. G., and Yim, S. C. S., "Seismic Response of Rotating Machines-Structures-RFBI Systems," *Earthquake Engineering and Structural Dynamics*, Vol. 29, No. 2, 2000, pp. 213–240.
doi:10.1002/(SICI)1096-9845(200002)29:2<213::AID-EQE900>3.0.CO;2-4

[11] Matsushita, O., Imashima, T., Hisanaga, Y., and Okubo, H., "Aseismic Vibration Control of Flexible Rotors Using Active Vibration Control," *Journal of Vibration and Acoustics*, Vol. 124, No. 1, 2002, pp. 49–57.
doi:10.1115/1.1423633

[12] Bachelet, L., Driot, N., and Ferraris, G., "Rotors Under Seismic Excitation: A Spectral Approach," *7th International Conference on Rotor Dynamics: IFToMM*, Vienna Univ. of Technology, Vienna, 25–28 Sept. 2006.

[13] Brown, M. A., and Shabana, A. A., "Application of Multibody Methodology to Rotating Shaft Problems," *Journal of Sound and Vibration*, Vol. 204, No. 3, 1997, pp. 439–457.
doi:10.1006/jsvi.1996.0868

[14] Lin, F., and Meng, G., "Study on the Dynamics of a Rotor in a Maneuvering Aircraft," *Journal of Vibration and Acoustics*, Vol. 125, No. 3, 2003, pp. 324–327.
doi:10.1115/1.1576422

[15] Duchemin, M., Berlioz, A., and Ferraris, G., "Dynamic Behaviour and Stability of a Rotor under Base Excitation," *Journal of Vibration and Acoustics*, Vol. 128, No. 5, 2006, pp. 576–585.
doi:10.1115/1.2202159

[16] Driot, N., Lamarque, C. H., and Berlioz, A., "Theoretical and Experimental Analysis of a Base-Excited Rotor," *Journal of Computational and Nonlinear Dynamics*, Vol. 1, No. 3, 2006, pp. 257–263.
doi:10.1115/1.2209648

[17] Cole, M. O. T., Keogh, P. S., and Burrows, C. R., "Vibration Control of a Flexible Rotor/Magnetic Bearing Subject to Direct Forcing and Base Motion Disturbances," *Journal of Mechanical Engineering Science: Proceedings of the Institution of Mechanical Engineers, Part C*, Vol. 212, No. 7, 1998, pp. 535–546.
doi:10.1243/0954406981521501

[18] Keogh, P. S., Sahinkaya, M. N., Burrows, C. R., and Prabhakar, S., "Wavelet Based Adaptation of *H*-Infinity Control in Rotor/Magnetic Bearing Systems," *7th International Conference on Rotor Dynamics: IFToMM*, Vienna Inst. of Technology, Vienna, 25–28 Sept. 2006.

[19] Nighil, M. C., Dutt, J. K., and Irretier, H., "Rotor Vibration Control with Electromagnetic Exciter," *7th International Conference on Rotor Dynamics, IFToMM*, Vienna Inst. of Technology, Vienna, 25–28 Sept. 2006.

[20] Janik, T. K., and Irretier, H., "New Excitation and Response Measurement Techniques for Modal Testing of Flexible Rotors," *Proceedings of the 5th International Conference on Rotor Dynamics*, Viewag, Brunswick, Germany, Sept. 1998, pp. 695–704.

[21] Janik, T. K., and Irretier, H., "Experimental Modal Analysis: A Tool for Unbalance Identification of Rotating Machines," *International Journal of Rotating Machinery*, Vol. 6, No. 1, 2000, pp. 11–18.

[22] Das, A. S., Nighil, M. C., Dutt, J. K., and Irretier, H., "Vibration Control and Stability Analysis of Rotor-Shaft System with Electromagnetic Exciters," *Mechanism and Machine Theory*, Vol. 43, No. 10, 2008, pp. 1295–1316.
doi:10.1016/j.mechmachtheory.2007.10.007

[23] Das, A. S., "Active Vibration Control of Flexible Rotors with Electromagnetic Actuator," Ph.D. Dissertation, Dept. of Mechanical Engineering, Indian Inst. of Technology, Kharagpur, India, 2009.

[24] Nelson, H. D., and McVaugh, J. M., "The Dynamics of Rotor Bearing System Using Finite Element," *Journal of Engineering for Industry*, Vol. 98, No. 2, 1976, pp. 593–600.

[25] Zorzi, E. S., and Nelson, H. D., "Finite Element Simulation of Rotor-Bearing Systems with Internal Damping," *Journal of Engineering for Power*, Vol. 99, Ser. 1, No. 1, 1977, pp. 71–76.

[26] Schweitzer, G., Bleuler, H., and Traxler, A., "Active Magnetic Bearings," published by the author, Zurich, 2003.

[27] Meirovitch, L., and Baruh, H., "Control of Self-adjoint Distributed Parameter Systems," *Journal of Guidance and Control*, Vol. 5, No. 1, 1982, pp. 60–66.
doi:10.2514/3.56140

J. Wei
Associate Editor